Multi-hump Collapsing Solutions in the Nonlinear Schrödinger Problem: Existence, Stability and Dynamics *

S. Jon Chapman†, M. Kavousanakis‡, E.G. Charalampidis§, I.G. Kevrekidis¶, and P.G. Kevrekidis‖

Abstract. In the present work we examine multi-hump solutions of the nonlinear Schrödinger equation in the blowup regime of the one-dimensional model with power law nonlinearity, bearing a suitable exponent of $\sigma > 2$. We find that families of such solutions exist for arbitrary pulse numbers, with all of them bifurcating from the critical case of $\sigma = 2$. Remarkably, all of them involve "bifurcations from infinity", i.e., the pulses come inward from an infinite distance as the exponent σ increases past the critical point. The position of the pulses is quantified and the stability of the waveforms is also systematically examined in the so-called "co-exploding frame". Both the equilibrium distance between the pulse peaks and the point spectrum eigenvalues associated with the multi-hump configurations are obtained as a function of the blowup rate G theoretically, and these findings are supported by detailed numerical computations. Finally, some prototypical dynamical scenarios are explored, and an outlook towards such multi-hump solutions in higher dimensions is provided.

Key words. Nonlinear Schrödinger equation, self-similarity, multi-hump waves, solitary wave, linear stability, WKB

MSC codes. 35Q55, 35B40, 34E20, 34D30

1. Introduction.

The nonlinear Schrödinger (NLS) model is undoubtedly one of the quintessential ones within the realm of dispersive nonlinear partial differential equations [3, 1, 36, 2]. It arises as a canonical or as an envelope model description in a diverse range of physical settings ranging from the evolution of optical beams in fibers and lasers [20, 24] to the description of atomic wavefunctions in ultracold Bose-Einstein condensates (BECs) [31, 30, 23], and from plasmas [25] to water waves [1].

While the focus of a large number of studies on the NLS model concerns the dynamics of its solitary wave solutions (either bright [24] or dark [23, 19]), the presence of *collapse* is

*Submitted to the editors October 23, 2025.

Funding: This work has been supported by the U.S. National Science Foundation under Grants DMS-2204782 (EGC), and PHY-2110030, PHY-2408988 and DMS-2204702 (PGK), and by the US National Science Foundation (IGK).

†Mathematical Institute, University of Oxford, AWB, ROQ, Woodstock Road, Oxford OX2 6GG (chapman@maths.ox.ac.uk.

‡School of Chemical Engineering, National Technical University of Athens, 15780, Athens, Greece (mihkavus@chemeng.ntua.gr).

§Department of Mathematics and Statistics, and Computational Science Research Center, San Diego State University, San Diego, CA 92182-7720, USA (echaralampidis@sdsu.edu).

¶Department of Chemical and Biomolecular Engineering &
Department of Applied Mathematics and Statistics, Johns Hopkins University, Baltimore, MD 21218, USA (yannisk@jhu.edu).

‖Department of Mathematics and Statistics, University of Massachusetts, Amherst MA 01003-4515, USA &
Department of Physics, University of Massachusetts, Amherst MA 01003, USA (kevrekid@umass.edu).

another key feature of the equation when nonlinear effects overcome dispersive ones. In this case, the relevant ground state solution to the NLS becomes (orbitally) unstable leading to the formation of singular solutions [36, 16]. From a physical perspective, the focusing nature of the problem induces self-similar collapse when the nonlinearity becomes "too strong" (e.g., considering a power nonlinearity $|u|^{2\sigma}u$ for a sufficiently large σ) [34, 12, 11], or when the dimensionality of the problem increases for fixed nonlinearity (e.g., considering a radially symmetric problem where the Laplacian reads $\Delta u = u_{rr} + (d-1)u_r/r$ for sufficiently large d [36, 27, 16, 9, 4]).

There has been a series of classic experiments that address relevant collapse features in NLS-type models, such as ones in nonlinear optics [28] observing the famous Townes soliton and its collapse, or more recent ones examining the collapse of structures with topological charge [39]. Intriguingly, after numerous years, experiments in other fields such as ultracold atomic systems have also been catching up, and have enabled alternative BEC realizations of Townes solitons in two separate recent experiments [5, 13]. Indeed, additional directions related to collapse have also been recently explored. These include the collapse of co-propagating beams with different wavelengths in the so-called two-color systems [35], as well as the consideration of vortical beams quenched from repulsive to attractive interactions in BECs and thus accordingly led to collapse [7].

It is some aspects of this very recent experimental endeavor of [7] that have motivated the present work. Indeed, in that work it was found that the original ring of atomic mass, prevented by the vortical structure from collapsing in the center of the condensate system, broke into a necklace structure consisting of individual (Townes-like) blobs which subsequently collapsed in the periphery of the ring pattern. This is also reminiscent of a scenario proposed earlier in the context of azimuthal modulational instability of a vortex solitary wave, e.g., in [10]. This scenario produces multiple concurrently collapsing structures, a setting that has, indeed, been theoretically considered earlier in the work of [29]. Arguably, the simplest setup enabling the study of such multi-bump states potentially leading to multiple concurrent blowups arises in one spatial dimension, i.e., $d = 1$. Indeed, the earlier work of [9] has partially examined such states in the realm of variable dimension d (i.e., used as a bifurcation parameter), which is rather unphysical (albeit interesting from a bifurcation perspective).

Here, motivated from our earlier studies which have considered the mathematically equivalent, yet more tractable setting of a variable nonlinear exponent σ, we revisit the examination of multi-pulse self-similarly exploding solutions. Firstly, we provide the mathematical setup (in section 2) that facilitates the numerical computation of these solutions, as a systematic bifurcation problem from the critical point of $\sigma d = 2$. [1] Varying the nonlinear exponent σ away from this critical point with fixed $d = 1$, we construct the full bifurcation diagrams of such multi-pulse collapsing states, observing all of them emerging from *infinity* at the respective bifurcation point. As part of our analytical considerations, we derive the asymptotic distance of the pulses as a function of the deviation from the critical point. Moreover, following up on the analysis of the stability of the single-bump collapsing branch that appeared in

[1] We remind the reader that at that critical point, it is well-known [36, 18] that the problem is conformally invariant and the collapsing solutions possess a blowup rate G that tends to 0 (in the model dynamics), in line with the findings reported below.

our earlier works [12, 11], here we provide a systematic spectral analysis of the multi-bump branches, examining how the number of unstable modes of the solutions grows as a function of the blowup rate G. The summary of our theoretical and numerical results is provided in section 3. Section 4 focuses on the details of the theoretical analysis for the steady problem; the corresponding stability analysis is considered in section 5. Indeed, we have identified some unexpected dependencies of the relevant eigenvalues and explain the systematics of how the relevant power laws on G emerge. Both the eigenvalues and the eigenvectors of the resulting instabilities are provided together with a number of direct numerical computations performed on the half domain. The latter showcase the destabilization of the relevant multi-humped solutions towards the single-humped one. Finally, we summarize our findings and conclusions in section 6, and discuss exciting avenues of future research emanating from the present work. A number of technical details concerning the numerical computations (involving, e.g., the comparison with alternative numerical approaches, as well as the dynamics in the full domain), and the analysis (such as the consideration of higher order terms in the bifurcation diagram) are presented in the Supplementary Material.

2. Theoretical and Numerical Setup. Our starting point for the examination of the multi-pulse collapse solutions will be the one-dimensional, nonlinear Schrödinger (NLS) equation with a power-law nonlinearity [12, 11] given by:

$$\mathrm{i}\frac{\partial\psi}{\partial z} + \frac{\partial^2\psi}{\partial x^2} + |\psi|^{2\sigma}\psi = 0, \tag{2.1}$$

where $\psi := \psi(x, z)$ is the complex-valued wavefunction, and σ, the strength of the (power-law) nonlinearity. The Hamiltonian associated with the NLS reads:

$$H = \int_{-\infty}^{\infty} \left(\left|\frac{\partial\psi}{\partial x}\right|^2 - \frac{1}{\sigma+1}|\psi|^{2\sigma+2} \right) \mathrm{d}x, \tag{2.2}$$

and satisfies:

$$\mathrm{i}\frac{\partial\psi}{\partial z} = \frac{\delta H}{\delta\psi^*}, \qquad \mathrm{i}\frac{\partial\psi^*}{\partial z} = -\frac{\delta H}{\delta\psi},$$

where $*$ stands for complex conjugation. It should be noted that H is finite for the Cauchy problem of the NLS.

The study of self-similar blowup solutions to the NLS necessitates the introduction of the so-called stretched variables:

$$\xi := \frac{x}{L}, \quad \tau := \int_0^z \frac{\mathrm{d}z'}{L^2(z')}, \quad \psi(x, z) := L^{-1/\sigma} v(\xi, \tau),$$

whose substitution to the NLS and Hamiltonian [cf. (2.1) and (2.2)] gives respectively

$$\mathrm{i}\frac{\partial v}{\partial\tau} + \frac{\partial^2 v}{\partial\xi^2} + |v|^{2\sigma}v - \mathrm{i}\xi L L_z \frac{\partial v}{\partial\xi} - \frac{\mathrm{i}LL_z}{\sigma}v = 0, \tag{2.3}$$

and

$$H = L^{-2/\sigma-2} \int_{-\infty}^{\infty} \left(\left|\frac{\partial v}{\partial\xi}\right|^2 - \frac{1}{\sigma+1}|v|^{2\sigma+2} \right) \mathrm{d}x.$$

We will refer to (2.3) as the NLS in the co-exploding frame hereafter, and define $G(\tau) \coloneqq -L\,L_z$ corresponding to the blowup rate. This way, (2.3) is conveniently written as:

$$\mathrm{i}\frac{\partial v}{\partial \tau} + \frac{\partial^2 v}{\partial \xi^2} + |v|^{2\sigma} v + \mathrm{i}G(\tau)\left(\xi\frac{\partial v}{\partial \xi} + \frac{1}{\sigma}v\right) = 0. \tag{2.4}$$

Finally, we factor out phase rotations via the transformation of the (complex-valued) field $v \mapsto \exp(\mathrm{i}\Lambda\tau)v$, and without loss of generality set $\Lambda = 1$; this can be done because a rescaling of independent and dependent variables, as well as a linear scaling of G by Λ can be used to scale out this parameter, as shown, e.g., in pp. 120–121 of [36]. Accordingly, we get:

$$\mathrm{i}\frac{\partial v}{\partial \tau} + \frac{\partial^2 v}{\partial \xi^2} + |v|^{2\sigma} v - v + \mathrm{i}G(\tau)\left(\xi\frac{\partial v}{\partial \xi} + \frac{1}{\sigma}v\right) = 0. \tag{2.5}$$

Self-similar blowup solutions to (2.5) are identified as *stationary* solutions therein, that is, $v(\xi,\tau) \mapsto v(\xi)$ when $\sigma > 2$ corresponding to the supercritical case for the one-dimensional NLS.

Indeed, we are able to numerically identify self-similar solutions by posing (2.5) on a computational yet finite spatial domain $[-K, K] \ni \xi$ supplemented with homogeneous Neumann boundary conditions, i.e., $v_\xi|_{\xi=\pm K} = 0,\ \forall\tau$. We consider a uniform spatial discretization with resolution (or nodal distance) $\Delta\xi$, and replace the spatial derivatives with respect to ξ in (2.5) with a centered, fourth-order accurate finite difference scheme. We further validated our numerical findings in this work by employing the finite element method as implemented in the open-source software `FreeFem++` [21] (see also section SM1 in the Supplementary Material).

Then, the identification of stationary solutions, i.e., self-similar ones to (2.5) involves the following twofold process. At first, we perform time-stepping using the BDF1 (i.e., backward Euler) scheme in order the self-similar dynamics to approach a stationary solution, i.e., $v(\xi,\tau) \mapsto v(\xi)$. We note that we corroborated our simulations here by using MATLAB's `ode23t` ODE solver (employing the trapezoidal method). Since the blowup rate G is an extra unknown to the problem, we close the system [i.e., select a unique among the one-parameter infinity of degenerate solutions] by imposing a pointwise, i.e., pinning condition of the form: $\mathrm{Im}\left[v(\xi=0,\tau)\right] = C \equiv \text{const.}$ stemming from the phase condition:

$$\int_{-K}^{K} \mathrm{Im}\left[v(\xi,\tau)\right] T(\xi)\mathrm{d}\xi = C, \tag{2.6}$$

where $T(\xi)$ is the so-called template function [32]. The pointwise condition we discussed above is obtained by Eq. (2.6) if we choose $T(\xi) = \delta(\xi)$. In most of our numerical computations, we set $C = 0$, thus seeking for a self-similar profile v satisfying: $\mathrm{Im}[v(0,\tau)] = 0$. We would like to note at this point that our numerical experimentation has suggested that pointwise conditions may be a bit restrictive (especially during parametric continuations), and thus as an alternative, we have also employed alternative phase conditions obtaining the same results in terms of the amplitude $|v|$ (and density $|v|^2$) of the solution although the real and imaginary parts of v may be different. This is not surprising as each approach respectively "pins down" a solution out of the group orbit of self-similar transformations.

Once the self-similar dynamics approaches a stationary profile $v(\xi)$ (and fixed blowup rate G, i.e., $G(\tau) \mapsto G \equiv \text{const.}$), the second step "corrects" the solution by seeking to identify it as a numerically exact solution using Newton's method. The waveform obtained from the self-similar dynamics is fed as an initial guess to the Newton solver, and it converges typically, within 2-3 iterations with very high accuracy. The resulting numerically exact solution (up to a prescribed accuracy) enables us subsequently to perform its spectral stability analysis in the co-exploding frame. For our stability computations and the results shown next, we use MATLAB's `eigs` (sparse matrix) eigenvalue solver. Our stability results are corroborated using also the FreeFEM's eigenvalue solver [21] (see also section SM1 in the Supplementary Material). The spectral stability results we obtained using both eigensolvers match precisely with each other. The above described process works very well for the fundamental (single hump) self-similar solution of (2.5).

Our primary focus, however, in this work is on multi-humped, self-similar solutions of the NLS for $\sigma > 2$. Since these solutions are dynamically unstable, an alternative approach is required, as self-similar dynamics will not (typically) converge to a stable stationary profile. To identify suitable profiles that can serve as initial guesses for Newton's method in solving the stationary two-point boundary-value problem (BVP), we adopt the approach (known as zero-Hamiltonian solutions method) introduced in [9] (see, also [16]). In brief, we consider the radially symmetric case (for $d = 1$ in [9]) that renders (2.5) now defined on the half-line, i.e., $[0, \infty) \ni \xi$ with v_+ being the symmetric solution. For computational purposes, we truncate the semi-infinite domain to a finite one $[0, K]$ with K typically being 200 to 1000. The stationary problem that we aim to solve is:

$$v_+'' - v_+ + \mathrm{i}G\left(\frac{1}{\sigma}v_+ + \xi v_+'\right) + |v_+|^{2\sigma}v_+ = 0, \tag{2.7}$$

supplemented with boundary conditions:

$$v_+'(0) = 0, \quad \mathrm{Im}[v_+(0)] = 0, \quad \left|Kv_+'(K) + (1 + i/G)\, v_+(K)\right| = 0, \tag{2.8}$$

where primes stand for (total) differentiation with respect to ξ.

The above BVP is solved by a combination of a shooting method and a (gradient-free) minimization technique that ultimately determines the unknown parameters $(\mathrm{Re}[v_+(0)], G)$, and thus the profile of interest. Indeed, starting from an initial guess $(\mathrm{Re}[v_+^{(0)}(0)], G^{(0)})$, the latter is treated as an initial condition to (2.7) which itself is viewed as an initial-value problem. Upon performing a forward integration in ξ up to $\xi = K$, we treat the boundary condition at $\xi = K$ in (2.8) as our objective function we want to minimize. For our purposes, we used MATLAB's `fminsearch` function (combined with the `ode23t` integrator), and corroborated our results using NAG's `e04jyf` minimization routine (and `dop853` integrator). Upon convergence, we determine $(\mathrm{Re}[v_+(0)], G)$ and the profile $v_+(\xi)$ of interest. Then, the solution $v(\xi)$ on $[-K, K]$ is constructed via symmetrization:

$$v(\xi) = \begin{cases} v_+(\xi), & \text{for } 0 \le \xi \le K \\ v_+(-\xi), & \text{for } -K \le \xi < 0, \end{cases} \tag{2.9}$$

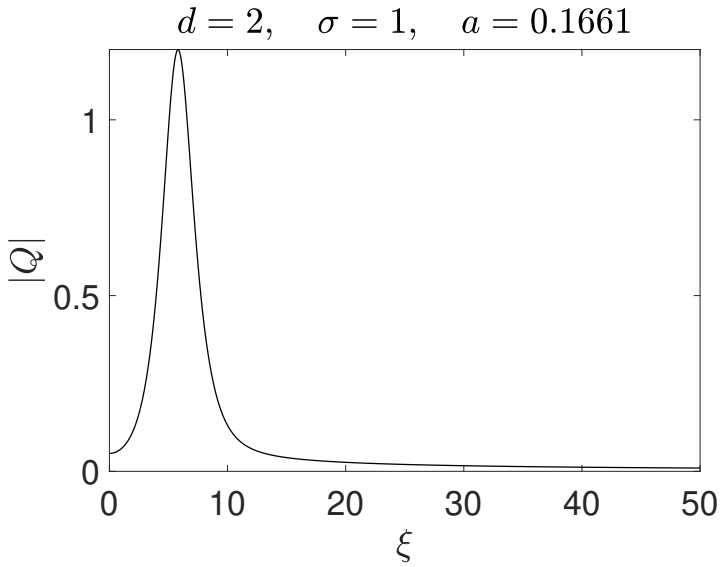

Figure 1: The amplitude $|v_+|$ of a double-humped solution to the BVP of (2.7)-(2.8) for $\sigma = 2.01$ and $K = 200$. The blowup rate for this solution is $G \approx 0.276$, and the bump, i.e., the highest in-amplitude peak appears at $\xi \approx 2.05$. To ease visualization, the amplitude $|v_+|$ is shown on $[0, 50]$. The inset displays a mangification of $|v_+|$ near the origin confirming the vanishing derivative of the amplitude.

and fed to our Newton solver in order to obtain the numerically exact solution. We performed a systematic scan of different initial guesses $(\mathrm{Re}[v_+^{(0)}(0)], G^{(0)})$ taken from the $(\mathrm{Re}[v_+(0)], G)$-plane, that gave us a plethora of multi-bump solutions to the NLS. Then, those were continued over σ parametrically by using pseudo-arclength continuation [26], thus obtaining branches of self-similar, multi-humped solutions, and constructing the respective bifurcation diagrams, i.e., G vs σ. For illustration purposes, Figure 1 displays an example of a double-humped solution to the boundary-value problem of (2.7)-(2.8) obtained on $[0, 200]$, where its amplitude $|v_+|$ is depicted as a function of ξ. The localized bump is located around $\xi \approx 2.05$. For this particular solution, the determined parameters are: $\mathrm{Re}[v_+(0)] = 0.4836$ and $G = 0.275549$.

3. Multihumped 1d self-similar solutions: Principal Existence and Stability Results.

3.1. Existence Results. Our prototypical results in terms of the existence of multi-pulse collapse states are presented in Figure 2 and Figure 3. More specifically, Figure 2 presents the spatial profiles of self-similar solutions with $n = 1$, 2, 3 and 4 humps, and blowup rate $G = 0.01$ ($\sigma > 2$). These profiles are stationary solutions of (2.5) obtained by setting $\frac{\partial v}{\partial \tau} = 0$. Indeed, we have identified even higher order states (not shown here), always coming in two sets of families (see also the relevant discussion of [9]), namely ones with odd numbers of peaks (featuring a peak at the center of symmetry of the configuration), as well as ones with an even number of peaks, *which are symmetric around a local minimum of the profile density.*

The variation of hump positions with blowup rate, G is displayed in Figure 3. This is

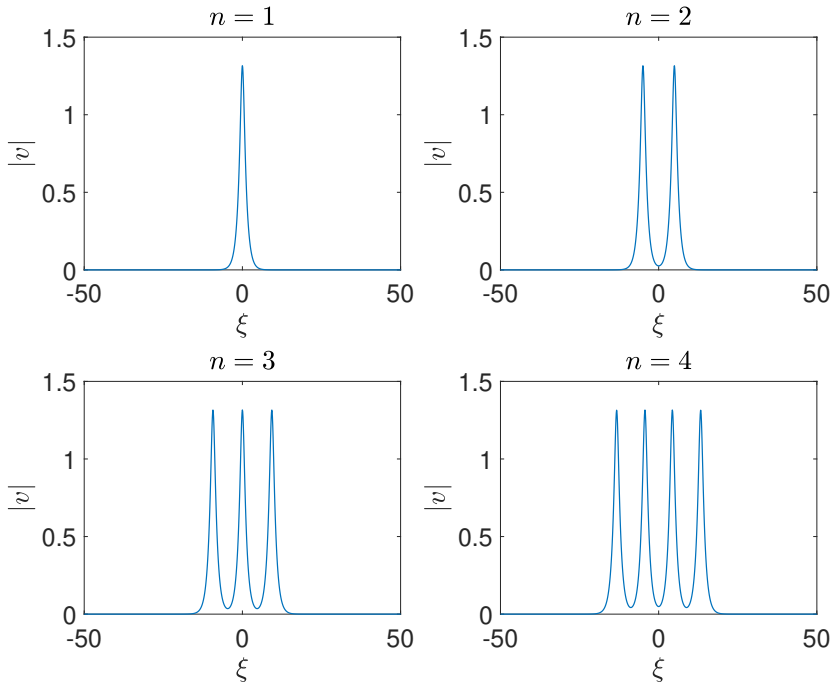

Figure 2: Comparison of self-similar blowup solutions with $n = 1, 2, 3$ and 4 humps for $G = 0.01$ and $K = 50$.

a point of contact and indeed of excellent agreement with our theoretical analysis that we now summarize (the analysis is presented in full detail in section 4). For the $n = 2$ case, the theoretical prediction for the equilibrium positions of the two-pulse configurations is given (symmetrically around 0) by the G-dependent expressions:

$$X_1 = -\frac{32}{\pi G^2} e^{-X_2+X_1}, \qquad X_2 = \frac{32}{\pi G^2} e^{-X_2+X_1},$$

so that $X_2 = -X_1 = X$, say, with

$$X = \frac{32}{\pi G^2} e^{-2X}.$$

The case of $n = 3$ equations leads our general expression detailed in section 4 to result in the predictions of:

$$X_1 = -\frac{32}{\pi G^2} e^{-X_2+X_1}, \qquad X_2 = \frac{32}{\pi G^2} \left(e^{-X_2+X_1} - e^{-X_3+X_2} \right), \qquad X_3 = \frac{32}{\pi G^2} e^{-X_3+X_2},$$

so that $X_3 = -X_1 = X$, say, $X_2 = 0$, with

$$X = \frac{32}{\pi G^2} e^{-X}.$$

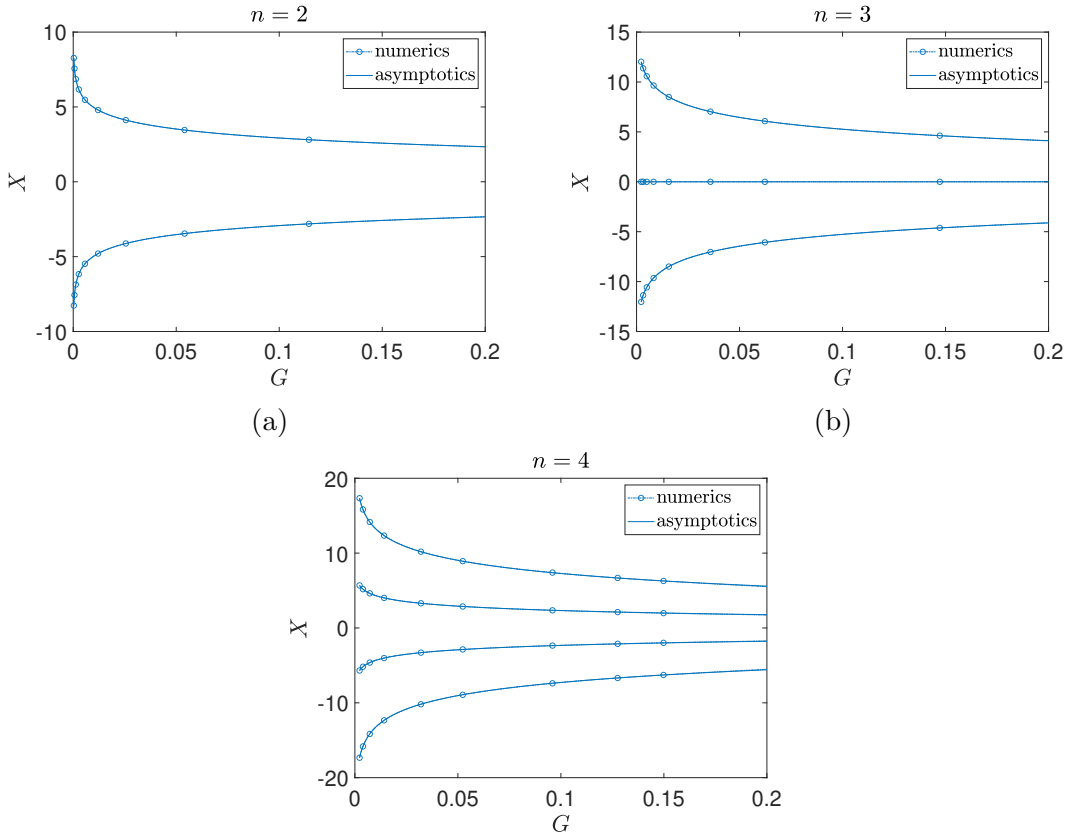

Figure 3: Variation of hump positions, X, with blowup rate, G for two ($n = 2$), three ($n = 3$) and four-humped ($n = 4$) self-similar solutions. The dash-dotted lines with open circles correspond to numerical solutions with $K = 50$. The solid lines represent the asymptotic prediction of the humps' positions.

Finally, among the cases shown in Figure 3, for $n = 4$, our theoretical predictions yield:

$$X_1 = -\frac{32}{\pi G^2} e^{-X_2+X_1}, \qquad X_2 = \frac{32}{\pi G^2}\left(e^{-X_2+X_1} - e^{-X_3+X_2}\right),$$
$$X_3 = \frac{32}{\pi G^2}\left(e^{-X_3+X_2} - e^{-X_4+X_3}\right), \qquad X_4 = \frac{32}{\pi G^2} e^{-X_4+X_3},$$

so that, with $X_3 = -X_2 = Y_1$, $X_4 = -X_1 = Y_2$, say, with

$$Y_1 = \frac{32}{\pi G^2}\left(e^{-2Y_1} - e^{-Y_2+Y_1}\right), \qquad Y_2 = \frac{32}{\pi G^2} e^{-Y_2+Y_1}.$$

We can observe that Figure 3 presents *excellent agreement* with the observed numerical results throughout the interval of consideration for the values of G. Similar predictions can be made for arbitrary values of n, as will be seen in section 4.

Moreover, having the positions of the pulses, we also derive in section 4 a systematic expression that provides the corresponding branch's bifurcation diagram, i.e., connects the blowup rate G with the nonlinearity power σ in line with our earlier calculation in [12]. More specifically:

$$\sigma - 2 = \frac{8\sigma}{n\pi}(\mathrm{e}^{2X_n} + \mathrm{e}^{-2X_1})\frac{\mathrm{e}^{-\pi/G}}{G}. \tag{3.1}$$

Note that with $n = 1$ and $X_1 = X_n = 0$ this reduces to the formula in [12], and also that we anticipate the solutions of (3.1) to satisfy $X_1 = -X_n$ so that

$$\sigma - 2 = \frac{16\sigma}{n\pi}\frac{\mathrm{e}^{2X_n - \pi/G}}{G}. \tag{3.2}$$

Figure 4 illustrates the dependence of G with the parameter σ for self-similar solutions of different numbers of humps, as obtained through our numerical computations. Among all self-similar profiles, only the single-humped ($n = 1$) solution with $G > 0$ is found to be stable (as will be discussed below). However, importantly for all the branches considered, we find again excellent agreement between the theoretical bifurcation curve prediction and the numerically obtained one. Only in the case of $n = 4$ can we detect a nearly imperceptible discrepancy at the level of the figure (at least with the eyeball metric) between theory and computation. While this discrepancy is modestly amplified as n becomes higher, it is clear that all the relevant branches are accurately captured by our asymptotics. Moreover, and quite importantly, this bifurcation analysis definitively shows that all of the relevant solutions emerge *concurrently* at the blowup threshold of $\sigma d = 2$. Indeed, as our position diagrams clearly indicate, the relevant waveforms constitute an example of "bifurcation from infinity", with the relevant pulses being "summoned back" (from an infinite) to a finite distance from each other as the blowup rate G increases.

3.2. Spectral Properties. We now turn to the examination of the stability features of each one of the branches that are identified herein. Before we do so, it is instructive to remind ourselves of the findings for the single-hump $n = 1$ branch as obtained earlier in [11]. In the relevant case, as the destabilization of the relevant solitonic branch proceeds (for the $G = 0$ solution), we have identified 6 point spectrum eigenvalues, i.e., 3-pairs near the origin. When we move to the co-exploding frame to obtain the self-similarly collapsing solution as a stationary state, it was argued in [11] that two exact eigenvalues can be computed ($\lambda = 2G$ and $\lambda = G$) associated with the symmetries of rescaling and of translation, respectively, in the case of the infinite domain. One more eigenvalue was found to stay at $\lambda = 0$, while 3 negative real eigenvalues slightly deviating from the opposites of the above values (as the system is no longer Hamiltonian) were also identified.

To consider the stability problem in further mathematical detail, we first perform a transformation: $v(\xi,\tau) = V(\xi,\tau)\mathrm{e}^{\mathrm{i}\tau - \mathrm{i}G(\tau)\xi^2/4}$ to turn our PDE problem to:

$$\mathrm{i}\frac{\partial V}{\partial \tau} + \frac{G'\xi^2}{4}V + \frac{\partial^2 V}{\partial \xi^2} + |V|^{2\sigma}V - V - \frac{\mathrm{i}(\sigma-2)G}{2\sigma}V + \frac{G^2\xi^2}{4}V = 0,$$

where $G' = \mathrm{d}G/\mathrm{d}\tau$.

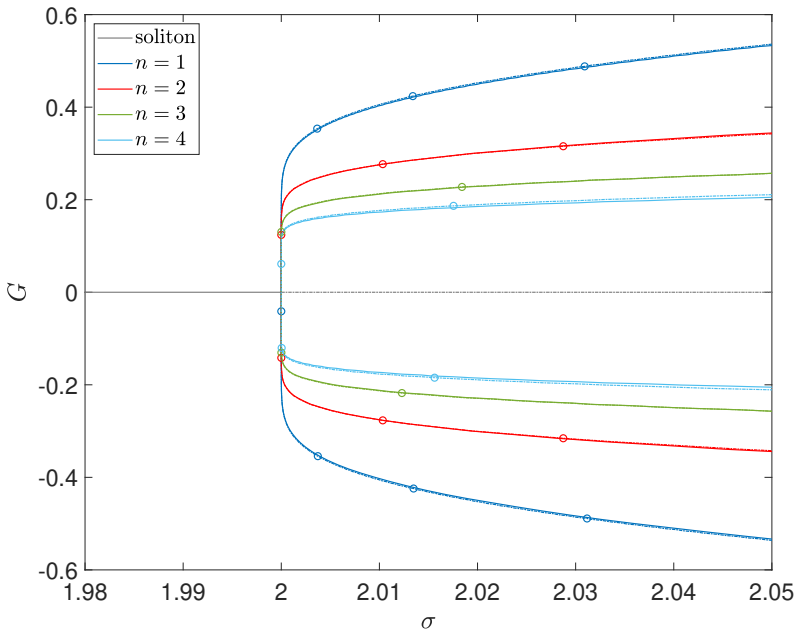

Figure 4: Variation of the blowup rate G as a function of σ for domain size, $K = 50$. The gray lines represent the blowup rate of soliton solutions ($G = 0$). Specifically, the solid gray line for $\sigma < 2$ corresponds to stable soliton solutions, while the dot-dashed gray line for $\sigma \geq 2$ indicates unstable soliton solutions. The blue line displays the blowup rate of $n = 1$-humped self-similar solutions. The blowup rates of self-similar solutions with $n = 2, 3, 4$ humps are depicted with red, green, and cyan lines, respectively. The dot-dashed lines with open circles represent the numerical computations, and the solid lines show the asymptotic prediction for the blowup rate G.

Then, the steady state solutions satisfy:

$$\frac{\mathrm{d}^2 V_s}{\mathrm{d}\xi^2} + |V_s|^{2\sigma} V_s - V_s - \frac{\mathrm{i}(\sigma-2)G}{2\sigma} V_s + \frac{G^2\xi^2}{4} V_s = 0, \tag{3.3}$$

with G constant equal to $G(\sigma)$. We linearize about the steady state by writing

$$V(\xi,\tau) = V_s(\xi) + \epsilon \left(f(\xi) \mathrm{e}^{\lambda\tau} + g^*(\xi) \mathrm{e}^{\lambda^*\tau} \right), \tag{3.4}$$

and accordingly obtain the eigenvalue problem

$$\mathrm{i}\lambda f + \frac{\mathrm{d}^2 f}{\mathrm{d}\xi^2} + \sigma |V_s|^{2\sigma-2} V_s^2 g + (\sigma+1)|V_s|^{2\sigma} f - f - \frac{\mathrm{i}(\sigma-2)G}{2\sigma} f + \frac{G^2\xi^2}{4} f = 0, \tag{3.5}$$

$$-\mathrm{i}\lambda g + \frac{\mathrm{d}^2 g}{\mathrm{d}\xi^2} + \sigma |V_s|^{2\sigma-2} (V_s^*)^2 f + (\sigma+1)|V_s|^{2\sigma} g - g + \frac{\mathrm{i}(\sigma-2)G}{2\sigma} g + \frac{G^2\xi^2}{4} g = 0. \tag{3.6}$$

Then, the two exact eigenvalues and their corresponding eigenvectors —for the infinite domain case— can be explicitly written as: $\lambda = 2G$,

$$f = \mathrm{i}V_s + G\left(\frac{V_s}{\sigma} + \xi\frac{\mathrm{d}V_s}{\mathrm{d}\xi} - \frac{\mathrm{i}G\xi^2 V_s}{2}\right), \quad g = -\mathrm{i}V_s^* + G\left(\frac{V_s^*}{\sigma} + \xi\frac{\mathrm{d}V_s^*}{\mathrm{d}\xi} + \frac{\mathrm{i}G\xi^2 V_s^*}{2}\right), \tag{3.7}$$

and $\lambda = G$,

$$f = \frac{\mathrm{d}V_s}{\mathrm{d}\xi} - \frac{\mathrm{i}G\xi V_s}{2}, \qquad g = \frac{\mathrm{d}V_s^*}{\mathrm{d}\xi} + \frac{\mathrm{i}G\xi V_s^*}{2}. \tag{3.8}$$

What we find in the case of the multi-bump collapse solutions is that the number of eigenvalues is effectively doubled when we consider two-pulse solutions instead of one. I.e., in the case of $n = 2$ we need to account for 12 point spectrum eigenvalues instead of 6. In the case of 3-pulse solutions this number rises to 18 and for $n = 4$ to 24. Remarkably (for us!) we have been able to fully categorize the eigenvalues of each one of these scenarios. Indeed, what we find in each case of n-pulse states is the following: the configuration ends up possessing *exactly* $n-1$ real eigenvalues that, to leading order, depend on the blowup rate in a predominantly square root form, i.e., $\lambda \propto G^{1/2}$. These eigenvalues, as will be shown below (through their eigenvectors), will be generally responsible for the breaking of the symmetry of the ($n \geq 2$) peaks, eventually leading to one peak dominating the blowup dynamics.

There are similarly $n+1$ real eigenvalues that end up with a dependence $\lambda \propto G$. Then, there exist $n-1$ pairs that end up being purely imaginary for an n-pulse state. Finally, one pair ends up near the origin. Given that, for each of the real eigenvalues, nearly the opposite λ is also (very close) to an eigenvalue, this accounts for $(n-1)+(n+1)+(n-1)+1$ i.e., $3n$ (approximate) pairs, i.e., $6n$ eigenvalues in total, which is what we observe for solutions consisting of n-copies of the original pulse. The spectra of the multi-humped self-similar solutions are illustrated in Figure 5 for $G = 0.01$. In all cases, one can observe that a vertical part of each spectrum aligns at $-G$, and the existence of real positive eigenvalues, the number of which changes with the number of humps, n. In particular, single-humped solutions have two dominant real eigenvalues, $n = 2$ solutions have four, $n = 3$ have six, and $n = 4$ have eight dominant real eigenvalues. All multi-humped self-similar solutions have two real eigenvalues $\lambda_1 \approx G$, and $\lambda_2 \approx 2G$ [rather than equal to G or $2G$ as our computations are affected by the finiteness of the computational domain]. The relevant count is fully in line with our qualitative discussion above.

Importantly, our methodology does not only provide the qualitative theoretical backdrop for the eigenvalue dependence on G. It provides, as will be evident in section 5, detailed quantitative estimates for the relevant eigenvalues. Moreover, it provides explicit predictions for the corresponding eigenfunctions. These can be seen in comparison to the numerically obtained eigenvectors in Figure 6 and to the corresponding numerical eigenvalues in Figure 7. The former are in excellent agreement with the numerical computations. For the latter, the $G^{1/2}$ dependence of $n-1$ real eigenvalues, and the G dependence of another $n+1$ ones is evident, and we see that for most of them the agreement is also quantitatively very accurate. For some of the eigenvalues, we observe a slight disparity (e.g., for λ_3 (green) one for the $n = 2$ case, λ_4 and λ_6 (black and red) for $n = 3$ and perhaps most notably λ_5 and λ_8 (purple and

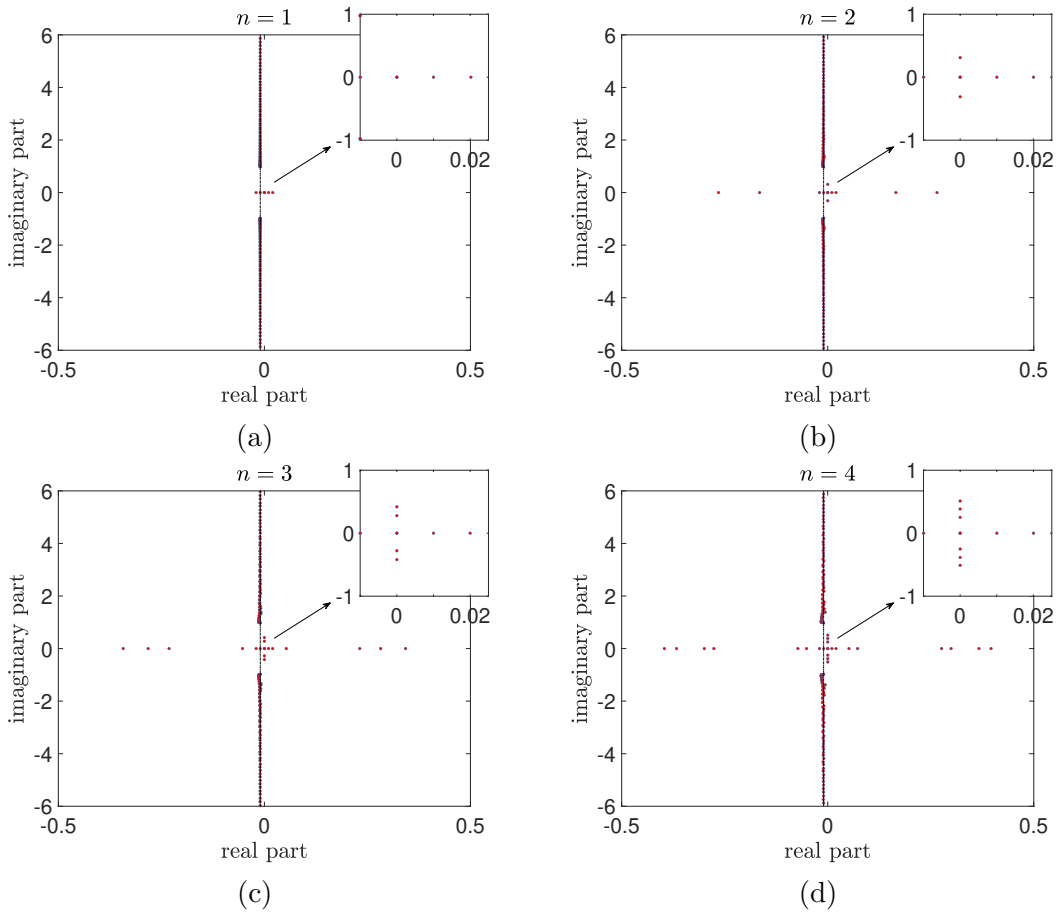

Figure 5: Single ($n = 1$) and multi-humped ($n = 2, 3, 4$) self-similar solution spectra for $G = 0.01$. The vertical part of the spectra align at $-G = -0.01$ for all cases (black dash-dotted lines). The insets illustrate real eigenvalues $\lambda \approx G$, $\lambda \approx 2G$, and eigenvalues with zero real part. One can observe the existence of a single conjugate pair of eigenvalues with zero real part for self-similar solutions with $n = 2$ humps, two pairs for $n = 3$, and three pairs for $n = 4$. For single-humped self-similar solutions there is only an eigenvalue at the origin.

pink ones) for $n = 4$). This is, however, chiefly true when the eigenvalues are sufficiently large and takes place due to higher order corrections not accounted for in our theory. Interestingly, for some other eigenvalues, these higher order corrections appear to be negligible, and the prediction remains highly accurate throughout the interval of considered values of G. At the moment, we do not have an explanation about why this takes place for some of the eigenvalues but not for others, other than to allude to reasons of symmetry. However, this is a potential interesting topic for further exploration.

3.3. Dynamics in the Self-similar Frame. Our methodology captures the associated dynamics in the rescaled $\xi - \tau$ spatio-temporal domain. In particular, we aim to validate the

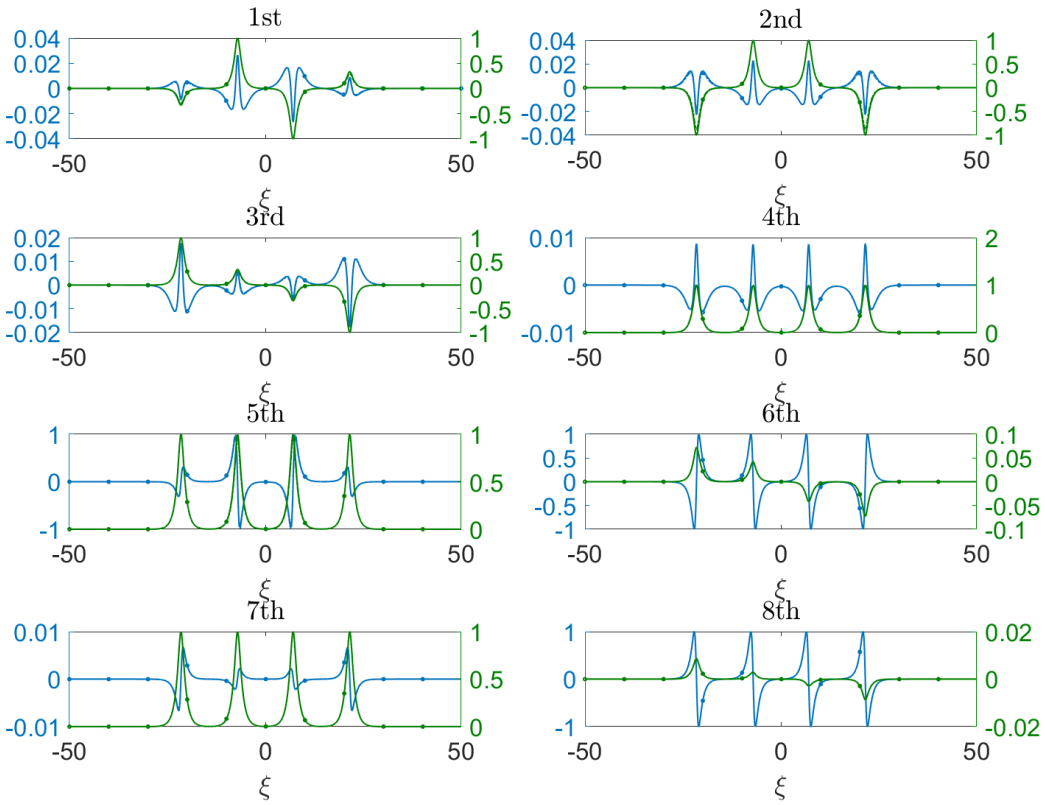

Figure 6: Eigenfunctions for 4-humped solutions and $G = 5\times10^{-4}$. Blue depicts the real parts and green corresponds to the imaginary parts. The numerical eigenfunctions are displayed with dash-dotted lines with open circles and asymptotic predictions (from section 5, truncated at $O(G)$) are displayed with solid lines. The two are practically indistinguishable from one another.

instability of multi-humped self-similar NLS solutions –discussed in the previous sections– in contrast to the stable single-humped self-similar solutions. For this purpose, we solve (2.5) in $\xi \in [0, K]$ with zero flux boundary conditions at both ends of the domain. The blowup rate, G, is computed by imposing a pinning condition, which "freezes" the imaginary part of v at $\xi = 0$ to a constant value, C, i.e.: $\mathrm{Im}\,[v(0,\tau)] = C$, in line with the above discussion. Time-stepping is performed by applying the backward Euler scheme, as also discussed above.

Figure 8(a)-(b) illustrates the evolution of unstable two-humped and three-humped self-similar solutions toward a stable single-humped self-similar state. The insets display the evolution of the blowup rate, G, with both cases achieving convergence after $\tau \approx 40$. For the two-humped case (Figure 8(a)), the initial condition is the self-similar solution at $\sigma = 2.011$ which is perturbed by decreasing σ by 10^{-4}, i.e., setting $\sigma = 2.0109$. For the three-humped

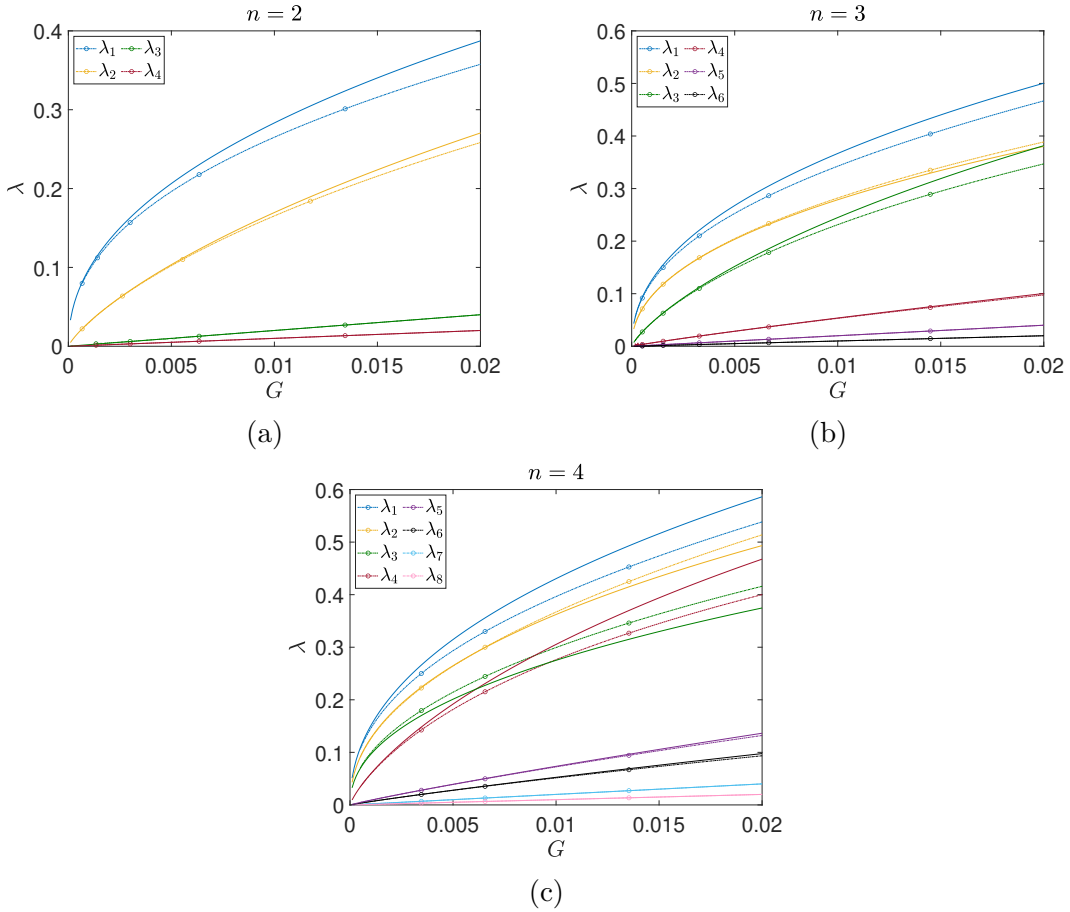

Figure 7: Variation of dominant real eigenvalues with blowup rate, G for (a) two ($n = 2$), (b) three ($n = 3$), and (c) four ($n = 4$) humped self-similar solutions. All multi-humped solutions share the $\lambda \approx G$ and $\lambda \approx 2G$ eigenvalues (λ_4 and λ_3 for $n = 2$, λ_6 and λ_5 for $n = 3$, and λ_8 and λ_7 for $n = 4$, respectively). Numerical computations for each eigenvalue are displayed with dash-dotted lines with open circles and asymptotic predictions are depicted with solid lines of the same color for each eigenvalue.

case (Figure 8(b)), we start with the self-similar solution computed at $\sigma = 2.011$ and perturb it by increasing σ by 10^{-4}, i.e., using $\sigma = 2.0111$ in the dynamical integration. In both cases, it is clear that asymptotically once some of the system's "mass" is ejected outward, the profiles can converge to the single-hump state.

However, it is important to note that convergence to the stable single-humped self-similar solution is not always guaranteed, and depends on the nature of the initial perturbation. For instance, reversing the sign of the σ perturbation in the two previous simulations prevents the dynamics from converging to a stable single-humped solution, as shown in Figure 9(a)-(b). Specifically, Figure 9(a) illustrates the evolution of the two-humped solution computed at

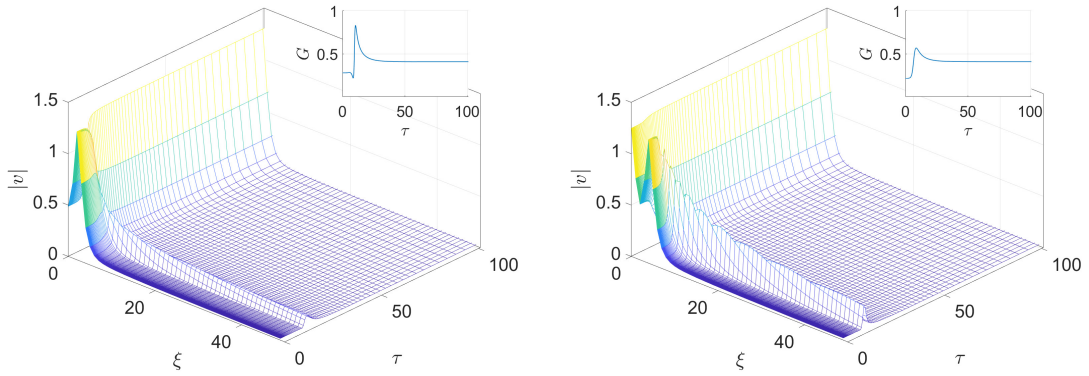

(a) (b)

Figure 8: Long time stability of single-humped self-similar solutions in dynamical simulations. (a) A two-humped self-similar solution, initially computed at $\sigma = 2.011$, evolves toward a stable single-humped self-similar solution after a slight decrease to $\sigma = 2.0109$. (b) A three-humped self-similar solution ($\sigma = 2.011$) transitions to a stable single-humped self-similar state when σ in increased to $\sigma = 2.0111$. The insets display the corresponding evolution of the blowup rate G. Simulations are performed in the domain $\xi \in [0, 50]$, with a nodal distance of $\Delta\xi = 0.002$.

$\sigma = 2.011$ and perturbed by increasing σ by 10^{-4} (i.e., $\sigma = 2.011$). Similarly, Figure 9(b) depicts the evolution of the three-humped solution, also computed at $\sigma = 2.011$, this time perturbed by decreasing σ to 2.0109. In both cases, the rescaled dynamics fail to reach a stable single-humped self-similar state. The relevant dynamics is also partially reminiscent of the work of [9] where the 3-hump solution [denoted as (1,2) therein] was found to be unstable, without signs of convergence to single-hump solution in its dynamics.

To further reinforce our statement we perform additional simulations, where the initial multi-humped state is perturbed along an unstable eigenvector associated with one of the dominant real eigenmodes. Here, we apply perturbations along the eigenmode corresponding to the largest real eigenvalue. In Figure 10(a)-(b), we present the spatio-temporal evolution of v starting from perturbed (a) two-humped, and (b) three-humped self-similar solutions computed at $\sigma = 2.001$. All different multi-modal self-similar states *are expected to evolve toward the same stable single-humped self-similar solution.* This is illustrated in Figure 10(c), where we show the initial state for each simulation (2-humped and 3-humped at $\tau = 0$) alongside the final, stable single-humped self-similar state at $\tau = 200$ for $\sigma = 2.001$. The converged blow-up rate ($G(\tau = 200) \approx 0.302$) is identical across all three simulations.

4. Detailed Asymptotic Analysis of the multi-hump steady state. We suppose that σ is exponentially close to 2 as $G \to 0$ (i.e. that $\sigma - 2 = o(G^k)$ for all $k > 0$; we will find that

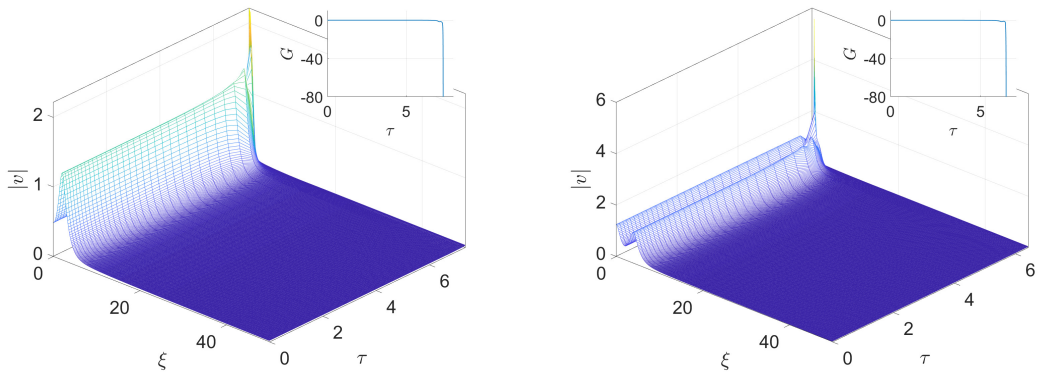

Figure 9: (a) Dynamical simulation starting from a two-humped self-similar solution at $\sigma = 2.011$; the σ value is now slightly increased to $\sigma = 2.0111$, and dynamics evolve away from the stable single-humped self-similar solution. (b) An initial three-humped self-similar solution computed at $\sigma = 2.011$ is now perturbed setting $\sigma = 2.0109$. Again, one observes that rescaled dynamics fail to converge to a stable self-similar state. The insets display the corresponding evolution of the blowup rate G. Simulations are performed in the domain $\xi \in [0, 50]$, with a nodal distance of $\Delta\xi = 0.002$.

$\sigma - 2 = O(\mathrm{e}^{-\pi/G}/G))$ so that, in steady state,

$$\frac{\mathrm{d}^2 V_s}{\mathrm{d}\xi^2} + |V_s|^4 V_s - V_s + \frac{G^2\xi^2}{4} V_s + \text{T.S.T.} = 0.$$

Here T.S.T. represents transcendentally small terms, that is, terms which are $o(G^k)$ as $G \to 0$ for all $k > 0$. We look for a general multi-hump solution, with humps located at $\xi = X_i(G)$ with $|X_i| \gg 1$, $i = 1, \ldots, n$, where we label such that $X_i < X_{i+1}$. We aim to determine the X_i along with the dependence of G on σ. We will find that each $X_i = O(\log G)$. By symmetry we expect to find $X_i = -X_{n+1-i}$, though we will not assume it. We use the pinning condition $\mathrm{Im}(V_s(0)) = 0$, for which we will find V_s is real to all algebraic orders in G.

For the single hump we found in [12] that the solution comprised a near field in the vicinity of the hump and a far field away from the hump. The far field contained a turning point, so there was also an inner region in the vicinity of the turning point which gave an exponentially-small reflection back towards the near field. This exponentially small component ultimately led to the relationship between σ and G describing the bifurcation. In the multi-hump case we will find that there is again a near field in the vicinity of each hump, along with new regions between adjacent humps. The far field, including the turning point, remains largely the same as in the single-hump case. We will detail the asymptotic solution in each region in turn, matching them to obtain the positions of the humps and the relationship between σ and G.

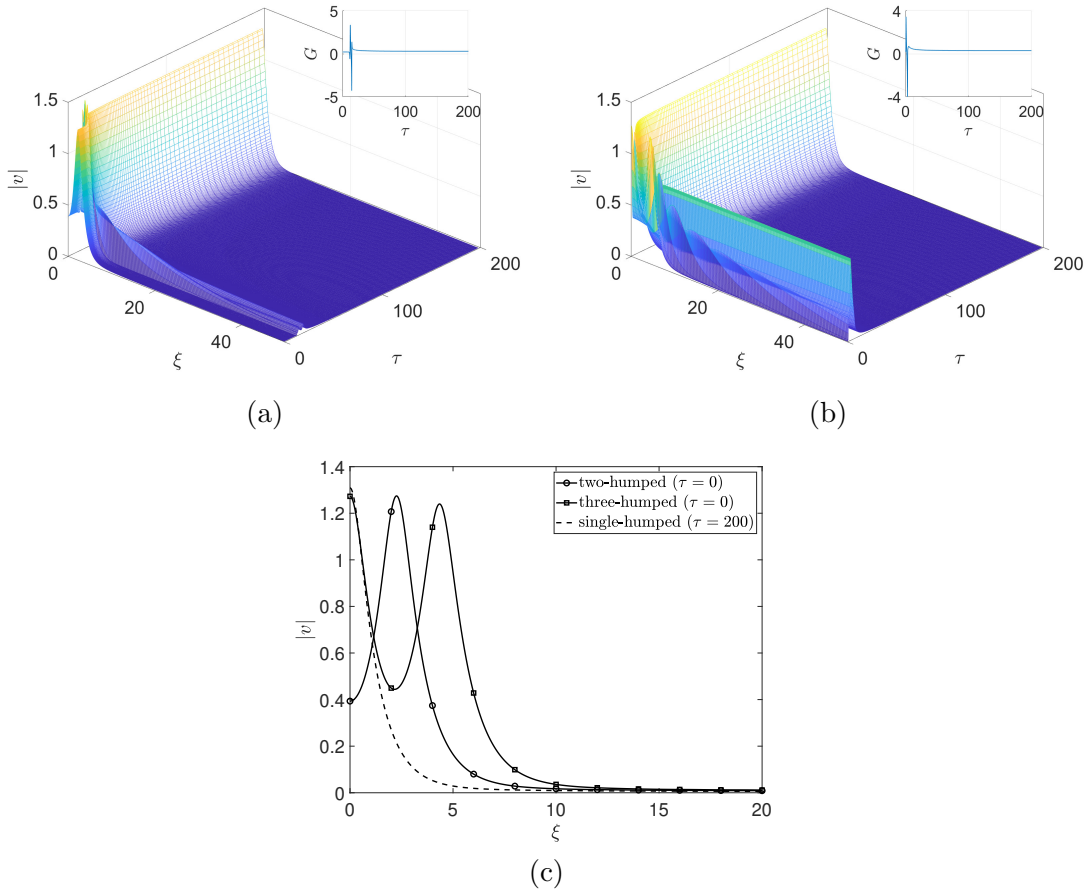

Figure 10: Dynamical simulations starting from (a) two-humped, and (b) three-humped self-similar solutions at $\sigma = 2.001$. By perturbing the initial condition along an unstable eigendirection (the one associated with the second largest real eigenvalue), the self-similar dynamics converged to the corresponding stable single-humped solution at large τ. The inset of each figure shows the corresponding evolution of the blow-up rate G. (c) The two different multi-humped states (2-humped and 3-humped) ultimately converge to the same stable single-humped self-similar profile (dashed line).

361 **4.1. Near field of the ith hump.** We write $\xi = X_i + x$ to give

362 (4.1)
$$\frac{\mathrm{d}^2 V_s}{\mathrm{d}x^2} + |V_s|^4 V_s - V_s + \frac{G^2 (x + X_i)^2}{4} V_s = 0.$$

363 Now expand

364 (4.2)
$$V_s = \sum_{n=0}^{\infty} G^{2n} V_n$$

to give the leading-order equation

$$\frac{\mathrm{d}^2 V_0}{\mathrm{d}x^2} + |V_0|^4 V_0 - V_0 = 0, \tag{4.3}$$

where we have assumed (and will verify a posteriori) that $G^2 X_i^2 \ll 1$. The relevant solution is the soliton,

$$V_0 = 3^{1/4}\,\mathrm{sech}^{1/2}(2x) = 3^{1/4}\,\mathrm{sech}^{1/2}\left[2(\xi - X_i)\right]. \tag{4.4}$$

4.2. Solution in between the humps. Consider the gap between X_i and X_{i+1}. In this region V_s is (algebraically) small, so we can neglect the nonlinear terms at leading order. Then, expanding again as in (4.2) gives

$$\frac{\mathrm{d}^2 V_0}{\mathrm{d}\xi^2} - V_0 = 0. \tag{4.5}$$

The inner solution (4.4) near X_{i+1} written in terms of ξ is

$$V_0 = 3^{1/4}\,\mathrm{sech}^{1/2}\left[2(\xi - X_{i+1})\right].$$

For large X_{i+1} with $\xi \ll X_{i+1}$ this is

$$V_0 \sim 12^{1/4}\mathrm{e}^{\xi - X_{i+1}}. \tag{4.6}$$

Similarly the inner solution near X_i written in terms of ξ is

$$V_0 = 3^{1/4}\,\mathrm{sech}^{1/2}\left[2(\xi - X_i)\right].$$

For large X_i with $X_i \ll \xi$ this is

$$V_0 \sim 12^{1/4}\mathrm{e}^{-\xi + X_i}. \tag{4.7}$$

Imposing these two matching conditions the solution of (4.5) for $X_i \ll \xi \ll X_{i+1}$ yields

$$V_0 = 12^{1/4}\mathrm{e}^{-\xi + X_i} + 12^{1/4}\mathrm{e}^{\xi - X_{i+1}}. \tag{4.8}$$

There is an exponentially small (in $X_i - X_{i+1}$) interaction term from each hump on the other. We will see that this term will match with the next term in the inner expansion, which is $O(G^2)$, so that $X_i - X_{i+1}$ will be logarithmically large in G. Writing (4.8) in terms of the inner variable $x = \xi - X_{i+1}$ gives

$$V_0 = 12^{1/4}\mathrm{e}^{x} + 12^{1/4}\mathrm{e}^{-x + X_i - X_{i+1}}; \tag{4.9}$$

thus the extra interaction term corresponds to an exponentially growing term leaving the inner region near X_{i+1}. Similarly, in terms of the inner variable $x = \xi - X_i$ we have

$$V_0 = 12^{1/4}\mathrm{e}^{-x} + 12^{1/4}\mathrm{e}^{x + X_i - X_{i+1}}, \tag{4.10}$$

again corresponding to an exponentially growing term leaving the inner region near X_i.

In the regions $\xi > X_n$ and $\xi < X_1$ there is no additional interaction term—the solution to (4.5) is a single exponential which decays at $\pm\infty$ respectively. We may include these regions in the general framework by adopting the convention that $X_0 = -\infty$, $X_{n+1} = \infty$, in which case (4.8) holds in these regions also.

4.3. Next order in the near field. Equating coefficients of G^2 in (4.1) gives

$$\frac{\mathrm{d}^2V_1}{\mathrm{d}x^2} + 5V_0^4V_1 - V_1 = -\frac{(x+X_i)^2}{4}V_0. \tag{4.11}$$

The homogeneous version of (4.11) is satisfied by V_0', so that there is a solvability condition. Multiplying by V_0' and integrating gives, on the LHS,

$$\int_{-R}^{R} \frac{\mathrm{d}V_0}{\mathrm{d}x}\left(\frac{\mathrm{d}^2V_1}{\mathrm{d}x^2} + 5V_0^4V_1 - V_1\right)\mathrm{d}x = \left[\frac{\mathrm{d}V_0}{\mathrm{d}x}\frac{\mathrm{d}V_1}{\mathrm{d}x} - \frac{\mathrm{d}^2V_0}{\mathrm{d}x^2}V_1\right]_{-R}^{R} + \int_{-R}^{R}\left(\frac{\partial^3V_0}{\partial x^3} + 5V_0^4\frac{\mathrm{d}V_0}{\mathrm{d}x} - \frac{\mathrm{d}V_0}{\mathrm{d}x}\right)V_1\,\mathrm{d}x,$$

so that the solvability condition is (when accounting for the vanishing of the integral term upon differentiation of the expression for V_0 in (4.3))

$$-\int_{-R}^{R}\frac{\mathrm{d}V_0}{\mathrm{d}x}\frac{(x+X_i)^2}{4}V_0\,\mathrm{d}x = \left[\frac{\mathrm{d}V_0}{\mathrm{d}x}\frac{\mathrm{d}V_1}{\mathrm{d}x} - \frac{\mathrm{d}^2V_0}{\mathrm{d}x^2}V_1\right]_{-R}^{R}. \tag{4.12}$$

Since V_0 is even the LHS may be simplified to

$$-X_i\int_{-R}^{R}\frac{\mathrm{d}V_0}{\mathrm{d}x}\frac{x}{2}V_0\,\mathrm{d}x = X_i\int_{-R}^{R}\frac{V_0^2}{4}\,\mathrm{d}x \to \frac{\sqrt{3}\,\pi X_i}{8} \text{ as } R\to\infty.$$

For the RHS we evaluate the boundary terms by matching with (4.9) and (4.10). As $x\to\infty$,

$$G^2V_1 \sim 12^{1/4}\mathrm{e}^{-X_{i+1}+X_i}\mathrm{e}^{x}, \qquad V_0 \sim 12^{1/4}\mathrm{e}^{-x}, \tag{4.13}$$

so that

$$\frac{\mathrm{d}V_0}{\mathrm{d}x}\frac{\mathrm{d}V_1}{\mathrm{d}x} - \frac{\mathrm{d}^2V_0}{\mathrm{d}x^2}V_1 \sim -4\sqrt{3}\,\frac{\mathrm{e}^{-X_{i+1}+X_i}}{G^2}.$$

Similarly, as $x\to-\infty$,

$$G^2V_1 \sim 12^{1/4}\mathrm{e}^{-X_i+X_{i-1}}\mathrm{e}^{-x}, \qquad V_0 \sim 12^{1/4}\mathrm{e}^{x}, \tag{4.14}$$

so that

$$\frac{\mathrm{d}V_0}{\mathrm{d}x}\frac{\mathrm{d}V_1}{\mathrm{d}x} - \frac{\mathrm{d}^2V_0}{\mathrm{d}x^2}V_1 \sim -4\sqrt{3}\,\frac{\mathrm{e}^{-X_i+X_{i-1}}}{G^2}.$$

Thus the solvability condition (4.12) is, as $R\to\infty$,

$$X_i = \frac{32}{\pi G^2}\left(\mathrm{e}^{-X_i+X_{i-1}} - \mathrm{e}^{-X_{i+1}+X_i}\right). \tag{4.15}$$

Equation (4.15) form a closed system of n equations for the n unknowns $X_1,\ldots,X_n$. It is relevant to note here that this set of equations (that is sometimes referred to as the —steady state form of— Toda lattice with nonzero masses) has appeared in other settings recently, such as, e.g., the case of N dark solitary waves in the presence of a parabolic confinement

applicable to atomic Bose-Einstein condensates [14]. In the latter case, the exponential tail-tail interaction of the solitary waves is balanced by the presence of the parabolic trap (onsite) effect on each of the solitary waves. On the other hand, here the linear effective potential stems from the role of the phase of the complex wavefunction past the critical point of collapse. It is especially relevant to mention in that context Lemma 5 of [14] which identifies the asymptotic form of the equilibrium solutions of (a rescaled form) Eq. (4.15). In the rescaling used therein, there exists a small parameter ε, which is proportional to G in the present notation. The lemma identifies the pairwise separation between the peaks as being logarithmic in ε with a doubly logarithmic correction. For the present case, we still need to identify σ, and to do so we need to consider the regions $\xi > X_n$ and $\xi < X_1$ more carefully.

4.4. Far field. Consider first the region $\xi > X_n$. When ξ is large the term $G^2\xi^2 V_s/4$ can no longer be neglected. Thus there is a different balance in the eqution in the far field. The solution is almost exactly the same as for the single-hump soliton reported in [12], so we merely sketch the analysis here.

We rescale $\xi = \rho/G$ to give

$$G^2\frac{\partial^2 V_s}{\partial \rho^2} + |V_s|^4 V_s - V_s + \frac{\rho^2}{4}V_s = 0.$$

Since V_s is exponentially small in the far field we can neglect the nonlinear term. We look for a WKB solution in the form

$$V_s \sim \mathrm{e}^{\phi(\rho)/G}\sum_{n=0}^{\infty} A_n(\rho)G^n. \tag{4.16}$$

At leading order this gives

$$(\phi')^2 = 1 - \frac{\rho^2}{4}.$$

Note the turning point at $\rho = 2$. For $\rho < 2$ the relevant solution is

$$\phi' = -\left(1 - \frac{\rho^2}{4}\right)^{1/2},$$

so that ϕ is decreasing (and V is exponentially decaying) as ρ increases. Let us fix the constant by writing

$$\phi = -\int_0^{\rho}\left(1 - \frac{\bar{\rho}^2}{4}\right)^{1/2}\mathrm{d}\bar{\rho}.$$

The leading-order amplitude equation is

$$2\phi' A_0' + \phi'' A_0 = 0,$$

so that

$$A_0 = \frac{a_0}{(-\phi')^{1/2}} = \frac{2^{1/2}\,a_0}{(4-\rho^2)^{1/4}}.$$

The constant a_0 is determined by matching with the near field solution in the vicinity of X_i. As $\rho \to 0$

$$\mathrm{e}^{\phi(\rho)/G} A_0 \sim a_0 \mathrm{e}^{-\rho/G}. \tag{4.17}$$

Since the right-most soliton is not positioned at the origin, the matching condition is slightly different to that in [12]. Writing (4.4) (or indeed (4.8)) in terms of ρ and expanding for small G gives

$$V_0 \sim 12^{1/4} \mathrm{e}^{-\rho/G + X_n}.$$

Matching with (4.17) gives

$$a_0 = 12^{1/4} \mathrm{e}^{X_n}.$$

Beyond the turning point, as $\rho \to \infty$ only the solution in which

$$\phi' = \mathrm{i} \left(\frac{\rho^2}{4} - 1 \right)^{1/2}$$

has a finite Hamiltonian. Thus for $\rho > 2$, the WKB solution is

$$V_s = \alpha \mathrm{e}^{\mathrm{i}\phi_2(\rho)/G} \sum_{n=0}^{\infty} A_n(\rho) (\mathrm{i}G)^n,$$

for some constant α, where

$$\phi_2 = \int_2^\rho \left(\frac{\bar{\rho}^2}{4} - 1 \right)^{1/2} \mathrm{d}\bar{\rho}, \qquad A_0(\rho) = \frac{2^{1/2} a_0}{(\rho^2 - 4)^{1/4}}.$$

The turning point causes an exponentially small reflection back into the near field. The solution in the turning point region is exactly the same as in [12], with the result that $\alpha = \mathrm{e}^{\mathrm{i}\pi/4}$ and the WKB solution in $\rho < 2$ is modified to

$$V_s = \mathrm{e}^{\phi(\rho)/G} \sum_{n=0}^{\infty} A_n(\rho) G^n + \gamma \mathrm{e}^{-\phi(\rho)/G} \sum_{n=0}^{\infty} A_n(\rho) (-G)^n, \qquad \rho < 2,$$

where, for an infinite domain,

$$\gamma = \frac{\mathrm{i}}{2} \mathrm{e}^{2\phi(2)/G} = \frac{\mathrm{i}}{2} \mathrm{e}^{-\pi/G}.$$

4.5. Matching back into the near field. We have found that the exponentially small correction to the far field in $0 < \rho < 2$ is

$$V_{\mathrm{exp}} = \gamma \mathrm{e}^{-\phi(\rho)/G} \sum_{n=0}^{\infty} A_n(\rho) (-G)^n.$$

As $\rho \to 0$

$$V_{\mathrm{exp}} \sim a_0 \gamma \mathrm{e}^{\rho/G}. \tag{4.18}$$

Writing $V_s = V_G + V_{\rm exp}$ where V_G is the original (multi-hump) algebraic expansion, and neglecting quadratic terms in $V_{\rm exp}$ but keeping now the term involving $\sigma - 2$ gives, noting that V_G is real, we obtain

$$\frac{\mathrm{d}^2 V_{\rm exp}}{\mathrm{d}\xi^2} + V_G^4(2V_{\rm exp}^* + 3V_{\rm exp}) - V_{\rm exp} + \frac{G^2\xi^2}{4}V_{\rm exp} = -2(\sigma-2)V_G^5 \log V_G + \frac{\mathrm{i}(\sigma-2)G}{2\sigma}V_G.$$

We separate into real and imaginary parts. Writing $V_{\rm exp} = U_{\rm exp} + \mathrm{i}W_{\rm exp}$ gives

$$\frac{\mathrm{d}^2 U_{\rm exp}}{\mathrm{d}\xi^2} + 5V_G^4 U_{\rm exp} - U_{\rm exp} + \frac{G^2\xi^2}{4}U_{\rm exp} = -2(\sigma-2)V_G^5 \log V_G, \tag{4.19}$$

$$\frac{\mathrm{d}^2 W_{\rm exp}}{\mathrm{d}\xi^2} + V_G^4 W_{\rm exp} - W_{\rm exp} + \frac{G^2\xi^2}{4}W_{\rm exp} = \frac{(\sigma-2)G}{2\sigma}V_G. \tag{4.20}$$

Note that V_G satisfies the homogeneous version of (4.20). The resulting solvability condition will determine σ. Unlike subsection 4.1-subsection 4.3, it is easiest now to consider this equation throughout the whole near-field region, rather than considering each hump separately. Multiplying (4.20) by V_G and integrating from $-R$ to R, while also using the equation satisfied by V_G, gives

$$\int_{-R}^{R}\left(V_G\frac{\mathrm{d}^2 W_{\rm exp}}{\mathrm{d}\xi^2} + V_G^5 W_{\rm exp} - V_G W_{\rm exp} + \frac{G^2\xi^2}{4}V_G W_{\rm exp}\right)\mathrm{d}\xi$$

$$= \left[V_G\frac{\mathrm{d}W_{\rm exp}}{\mathrm{d}\xi} - W_{\rm exp}\frac{\mathrm{d}V_G}{\mathrm{d}\xi}\right]_{-R}^{R} + \int_{-R}^{R}\left(W_{\rm exp}\frac{\mathrm{d}^2 V_G}{\mathrm{d}\xi^2} + V_G^5 W_{\rm exp} - V_G W_{\rm exp} + \frac{G^2\xi^2}{4}V_G W_{\rm exp}\right)\mathrm{d}\xi$$

$$= \left[V_G\frac{\mathrm{d}W_{\rm exp}}{\mathrm{d}\xi} - W_{\rm exp}\frac{\mathrm{d}V_G}{\mathrm{d}\xi}\right]_{-R}^{R} = \frac{(\sigma-2)G}{2\sigma}\int_{-R}^{R} V_G^2\,\mathrm{d}x. \tag{4.21}$$

As $R \to \infty$ we evaluate the boundary terms by matching using (4.18). We find

$$V_G(R)\frac{\mathrm{d}W_{\rm exp}}{\mathrm{d}x}(R) - W_{\rm exp}(R)\frac{\mathrm{d}V_G}{\mathrm{d}x}(R) = 2\sqrt{3}\,\mathrm{e}^{2X_n}\mathrm{e}^{-\pi/G} \qquad \text{as } R\to\infty.$$

A similar calculation in $\xi < X_1$ shows that

$$V_G(-R)\frac{\mathrm{d}W_{\rm exp}}{\mathrm{d}x}(-R) - W_{\rm exp}(-R)\frac{\mathrm{d}V_G}{\mathrm{d}x}(-R) = -2\sqrt{3}\,\mathrm{e}^{-2X_1}\mathrm{e}^{-\pi/G} \qquad \text{as } R\to\infty.$$

The dominant contribution to the RHS of (4.21) comes from each of the humps, since V_G is $O(G^2)$ in between the humps. Since

$$\int_{-\infty}^{\infty} V_0(x)^2\,\mathrm{d}x = \frac{\sqrt{3}\,\pi}{2},$$

we find, finally

$$\sigma - 2 = \frac{8\sigma}{n\pi}(\mathrm{e}^{2X_n} + \mathrm{e}^{-2X_1})\frac{\mathrm{e}^{-\pi/G}}{G}. \tag{4.22}$$

Note that with $n = 1$ and $X_1 = X_n = 0$ this reduces to the formula in [12], and also that we anticipate the solutions of (4.22) to satisfy $X_1 = -X_n$ so that

$$\sigma - 2 = \frac{16\sigma}{n\pi}\frac{\mathrm{e}^{2X_n - \pi/G}}{G}. \tag{4.23}$$

5. Detailed Asymptotic Analysis of the multi-hump eigenvalues. Since V_s is real to all orders, and σ is exponentially close to 2, we may write the linearization problem of (3.5)-(3.6) as

$$\mathrm{i}\lambda f + \frac{\mathrm{d}^2 f}{\mathrm{d}\xi^2} + 2V_s^4 g + 3V_s^4 f - f + \frac{G^2\xi^2}{4} f = \text{T.S.T.}, \tag{5.1}$$

$$-\mathrm{i}\lambda g + \frac{\mathrm{d}^2 g}{\mathrm{d}\xi^2} + 2V_s^4 f + 3V_s^4 g - g + \frac{G^2\xi^2}{4} g = \text{T.S.T.}. \tag{5.2}$$

We aim to find asymptotic approximations to the real eigenvalues found numerically in section 3. Since V_s is real to all orders, when λ is real we may write $g = f^* + \text{T.S.T.}$, so that

$$\mathrm{i}\lambda f + \frac{\mathrm{d}^2 f}{\mathrm{d}\xi^2} + 2V_s^4 f^* + 3V_s^4 f - f + \frac{G^2\xi^2}{4} f = \text{T.S.T.}. \tag{5.3}$$

Anticipating that λ is small when G is small, the leading-order eigenfunctions satisfy

$$\frac{\mathrm{d}^2 f_0}{\mathrm{d}\xi^2} + 2V_0^4 f_0^* + 3V_0^4 f_0 - f_0 = 0. \tag{5.4}$$

There are two solutions to this equation, namely

$$f_0 = \frac{\mathrm{d}V_0}{\mathrm{d}\xi}, \qquad f_0 = \mathrm{i}V_0.$$

For a multi-hump steady state we may take a different multiple of $\mathrm{d}V_0/\mathrm{d}\xi$ or $\mathrm{i}V_0$ at each hump. We begin in subsection 5.1 by analysing the eigenfunctions which are proportional to $\mathrm{i}V_0$ near each hump, which give the dominant eigenvalues. We then, in subsection 5.2, analyse those eigenfunctions which are proportional to $\mathrm{d}V_0/\mathrm{d}\xi$, which are much more difficult to find.

Throughout the analysis we will encounter inhomogeneous versions of (5.4) in the form

$$\frac{\mathrm{d}^2 f}{\mathrm{d}x^2} + 2V_0^4 f^* + 3V_0^4 f - f = \rho. \tag{5.5}$$

Since the imaginary part of the homogeneous equation has the nontrivial solution V_0, and the real part of the homogeneous equation has the nontrivial solution $\mathrm{d}V_0/\mathrm{d}x$, there are two solvability conditions on (5.5), namely,

$$\mathrm{Im}\left[\frac{\mathrm{d}f}{\mathrm{d}x}V_0 - f\frac{\mathrm{d}V_0}{\mathrm{d}x}\right]_{-R}^{R} = \int_{-R}^{R} \mathrm{Im}(\rho)V_0\,\mathrm{d}x, \tag{5.6}$$

$$\mathrm{Re}\left[\frac{\mathrm{d}f}{\mathrm{d}x}\frac{\mathrm{d}V_0}{\mathrm{d}x} - f\frac{\mathrm{d}^2 V_0}{\mathrm{d}x^2}\right]_{-R}^{R} = \int_{-R}^{R} \mathrm{Re}(\rho)\frac{\mathrm{d}V_0}{\mathrm{d}x}\,\mathrm{d}x, \tag{5.7}$$

for all R. We will of course be interested in the limit $R \to \infty$.

5.1. Perturbation of $f = \mathrm{i}V_0$: eigenvalues of $O(G^{1/2})$. Guided by our numerical results let us anticipate that $\lambda = O(G^{1/2})$ and write $\lambda = G^{1/2}\lambda_1$. We will perturb in powers of $G^{1/2}$. The expansion has a similar structure to that of section 4—there are inner regions in the vicinity of each hump, and outer regions between humps, which much be matched together to give λ.

536 **5.1.1. Inner expansion near the ith hump.** With $\xi = X_i + x$, we expand

537 $$f = b_i \sum_{k=0}^{\infty} G^{k/2} f_k,$$

538 with $f_0 = \mathrm{i}V_0$. Here b_i is the amplitude of the eigenfunction near the i th hump. As mentioned
539 above, for a single hump this would scale out of the problem, but for multiple humps the
540 coefficient of $\mathrm{i}V_0$ may be different at different humps. We must determine b_i as part of the
541 problem, but this will only happen once we consider the interaction between humps in §5.1.2.
542 In the end we will find a homogeneous linear system (5.18) for the b_i, which will determine
543 the eigenvalue λ_1, along with b_i as the components of the corresponding eigenvector.
544 At $O(G^{1/2})$ we have

545 $$\frac{\mathrm{d}^2 f_1}{\mathrm{d}x^2} + V_0^4(2f_1^* + 3f_1) - f_1 = \lambda_1 V_0.$$

546 The solvability conditions (5.6), (5.7) are automatically satisfied, so that λ_1 is undetermined,
547 and

548 $$f_1 = \lambda_1 \left(\frac{V_0}{4} + \frac{x}{2}\frac{\mathrm{d}V_0}{\mathrm{d}x} \right).$$

549 At $O(G)$ we find [2]

550 $$\frac{\mathrm{d}^2 f_2}{\mathrm{d}x^2} + V_0^4(2f_2^* + 3f_2) - f_2 = -\mathrm{i}\lambda_1^2 \left(\frac{V_0}{4} + \frac{x}{2}\frac{\mathrm{d}V_0}{\mathrm{d}x} \right).$$

551 Again the solvability conditions (5.6), (5.7) are automatically satisfied, so that λ_1 is still
552 undetermined, and the solution is

553 $$f_2 = -\frac{\mathrm{i}\lambda_1^2}{8} x^2 V_0.$$

554 At $O(G^{3/2})$ we find

555 $$\frac{\mathrm{d}^2 f_3}{\mathrm{d}x^2} + V_0^4(2f_3^* + 3f_3) - f_3 = -\frac{\lambda_1^3 x^2}{8} V_0.$$

556 As before, the solvability conditions are automatically satisfied, and the solution is

557 $$f_3 = \frac{\lambda_1^3}{2}\hat{V}_1, \qquad g_3 = \frac{\lambda_1^3}{2}\hat{V}_1,$$

558 where $\hat{V}_1$ satisfies

559 $$\frac{\mathrm{d}^2 \hat{V}_1}{\mathrm{d}x^2} + 5V_0^4 \hat{V}_1 - \hat{V}_1 = -\frac{x^2 V_0}{4}, \qquad \hat{V}_1 \to 0 \text{ as } x \to \pm\infty,$$

560 that is, $\hat{V}_1$ is the next term in the expansion of the standard single hump solution [12] (i.e.
561 not accounting for the shift in origin). At $O(G^2)$ we find

562 (5.8) $$\frac{\mathrm{d}^2 f_4}{\mathrm{d}x^2} + V_0^4(2f_4^* + 3f_4) - f_4 = -\frac{\mathrm{i}\lambda_1^4}{2}\hat{V}_1 - \frac{\mathrm{i}(x + X_i)^2}{4} V_0 - 4\mathrm{i}V_1 V_0^4.$$

[2] Really we should expand λ (and b_i) in powers of G, so that there would be additional terms on the RHS due to λ_2. However, these terms will simply mirror the terms involving λ_1 at the previous order, and we can ignore them if we are only interested in the leading approximation of the eigenvalue.

Here at last the solvability condition (5.6) is not automatically satisfied, and will determine λ_1. Note that V_1 grows exponentially as $x \to \pm\infty$ (in contrast to $\hat{V}_1$)—see (4.13), (4.14)—so that we must be careful in evaluating the solvability condition. Multiplying (4.11) by V_0 and integrating gives

$$\begin{aligned} -\int_{-R}^{R} \frac{(x+X_i)^2}{4} V_0^2 \,\mathrm{d}x &= \int_{-R}^{R} \left(\frac{\mathrm{d}^2 V_1}{\mathrm{d}x^2} + 5V_0^4 V_1 - V_1 \right) V_0 \,\mathrm{d}x \\ &= \int_{-R}^{R} \left(\frac{\mathrm{d}^2 V_0}{\mathrm{d}x^2} + 5V_0^5 - V_0 \right) V_1 \,\mathrm{d}x + \left[\frac{\mathrm{d}V_1}{\mathrm{d}x} V_0 - V_1 \frac{\mathrm{d}V_0}{\mathrm{d}x} \right]_{-R}^{R} \\ &= \int_{-R}^{R} 4V_0^5 V_1 \,\mathrm{d}x + \left[\frac{\mathrm{d}V_1}{\mathrm{d}x} V_0 - V_1 \frac{\mathrm{d}V_0}{\mathrm{d}x} \right]_{-R}^{R}. \end{aligned}$$

Thus the solvability conditions on (5.8) may be written as

$$\mathrm{Im} \left[\frac{\mathrm{d}f_4}{\mathrm{d}x} V_0 - f_4 \frac{\mathrm{d}V_0}{\mathrm{d}x} \right]_{-R}^{R} = -\frac{\lambda_1^4}{2} \int_{-R}^{R} \hat{V}_1 V_0 \,\mathrm{d}x + \left[\frac{\mathrm{d}V_1}{\mathrm{d}x} V_0 - V_1 \frac{\mathrm{d}V_0}{\mathrm{d}x} \right]_{-R}^{R} \tag{5.9}$$

$$\mathrm{Re} \left[\frac{\mathrm{d}f_4}{\mathrm{d}x} \frac{\mathrm{d}V_0}{\mathrm{d}x} - f_4 \frac{\mathrm{d}^2 V_0}{\mathrm{d}x^2} \right]_{-R}^{R} = 0. \tag{5.10}$$

The boundary terms on the RHS can be evaluated using (4.13), (4.14). To evaluate the boundary terms on the LHS we need to consider f in the region between humps.

5.1.2. In between the humps. Consider the gap between X_i and X_{i+1}. In this region $V_s = O(G^2 \log G)$ so that we can neglect the nonlinear term. Thus

$$\mathrm{i}G^{1/2}\lambda_1 f + \frac{\mathrm{d}^2 f}{\mathrm{d}\xi^2} - f + \frac{G^2\xi^2}{4} f = O(fG^8 \log^4 G). \tag{5.11}$$

Expanding

$$f = \sum_{k=0}^{\infty} G^{k/2} f_k,$$

gives

$$\frac{\mathrm{d}^2 f_0}{\mathrm{d}\xi^2} - f_0 = 0, \tag{5.12}$$

at leading order. Matching requires

$$f_0 \sim 12^{1/4} \mathrm{i} b_{i+1} \mathrm{e}^{\xi - X_{i+1}} \quad \text{as } \xi \to X_{i+1}, \qquad f_0 \sim 12^{1/4} \mathrm{i} b_i \mathrm{e}^{-\xi + X_i} \quad \text{as } \xi \to X_i.$$

Thus

$$f_0 = 12^{1/4} \mathrm{i} b_{i+1} \mathrm{e}^{\xi - X_{i+1}} + 12^{1/4} \mathrm{i} b_i \mathrm{e}^{-\xi + X_i}.$$

In terms of $\xi = X_{i+1} + x$ this is

$$f_0 = 12^{1/4} \mathrm{i} b_{i+1} \mathrm{e}^{x} + 12^{1/4} \mathrm{i} b_i \mathrm{e}^{-x + X_i - X_{i+1}}.$$

Since $\mathrm{e}^{X_i - X_{i+1}} = O(G^2)$ the additional term must match with $G^2 f_4$ from the $(i+1)$th hump solution, giving

$$b_{i+1} f_4 G^2 \sim 12^{1/4} \mathrm{i} b_i \mathrm{e}^{-x + X_i - X_{i+1}}, \tag{5.13}$$

as $x \to -\infty$. Similarly, in terms of $\xi = X_i + x$,

$$f_0 = 12^{1/4} \mathrm{i} b_{i+1} \mathrm{e}^{x + X_i - X_{i+1}} + 12^{1/4} \mathrm{i} b_i \mathrm{e}^{-x},$$

giving the matching condition on the i th hump solution

$$b_i f_4 G^2 \sim 12^{1/4} \mathrm{i} b_{i+1} \mathrm{e}^{x + X_i - X_{i+1}}, \tag{5.14}$$

as $x \to \infty$. Under our convention that $X_0 = -\infty$, $X_{n+1} = \infty$ equations (5.13), (5.14) can be extended to include $i = 0$ and $i = n$, respectively.

5.1.3. Solvability condition. We now have enough information to evaluate the solvability conditions (5.9), (5.10). Using (5.13), (5.14), (4.13) and (4.14) gives

$$\lim_{R\to\infty} \mathrm{Re} \left[\frac{\mathrm{d}f_4}{\mathrm{d}x} \frac{\mathrm{d}V_0}{\mathrm{d}x} - f_4 \frac{\mathrm{d}^2 V_0}{\mathrm{d}x^2} \right]_{-R}^{R} = 0, \tag{5.15}$$

$$\lim_{R\to\infty} \mathrm{Im} \left[b_i \frac{\mathrm{d}f_4}{\mathrm{d}x} V_0 - b_i f_4 \frac{\mathrm{d}V_0}{\mathrm{d}x} \right]_{-R}^{R} = 4\sqrt{3}\, \mathrm{i} b_{i+1} \frac{\mathrm{e}^{X_i - X_{i+1}}}{G^2} + 4\sqrt{3}\, \mathrm{i} b_{i-1} \frac{\mathrm{e}^{X_{i-1} - X_i}}{G^2}, \tag{5.16}$$

$$\lim_{R\to\infty} \left[\frac{\mathrm{d}V_1}{\mathrm{d}x} V_0 - V_1 \frac{\mathrm{d}V_0}{\mathrm{d}x} \right]_{-R}^{R} = 4\sqrt{3} \frac{\mathrm{e}^{X_i - X_{i+1}}}{G^2} + 4\sqrt{3} \frac{\mathrm{e}^{X_{i-1} - X_i}}{G^2}. \tag{5.17}$$

Thus, letting $R \to \infty$, (5.10) is satisfied, and, since

$$\int_{-\infty}^{\infty} \hat{V}_1 V_0 \, \mathrm{d}x = \frac{\sqrt{3}\, \pi^3}{256},$$

the remaining condition (5.9) is

$$\frac{b_i \lambda_1^4 \pi^3}{2048} = (b_i - b_{i+1}) \frac{\mathrm{e}^{X_i - X_{i+1}}}{G^2} + (b_i - b_{i-1}) \frac{\mathrm{e}^{X_{i-1} - X_i}}{G^2}, \qquad i = 1, \ldots, n. \tag{5.18}$$

Equation (5.18) is a set of n homogeneous linear equations for the n coefficients b_i, $i = 1, \ldots, n$. For a nontrivial solution the determinant must vanish, and it is this condition that determines the eigenvalue λ_1: $\lambda_1^4 \pi^3 / 2048$ is an eigenvalue of this system, with b_i the components of the corresponding eigenvector. Note that $b_i = b$ for all i, $\lambda_1 = 0$ is a solution of (5.18) for any n. This corresponds to global phase invariance, with corresponding eigenvalue $\lambda = 2G$ (we would need to include λ_2 and proceed to higher orders to see that through this expansion, but fortunately we have an exact eigenfunction for $\lambda = 2G$ in (3.7)). Thus we expect that there are $n - 1$ remaining eigenvalues which are $O(G^{1/2})$. Note also that the eigenvalues appear in pairs—for each positive eigenvalue there is a corresponding negative eigenvalue with the same (leading order) weights b_i.

5.1.4. Examples.

Two humps:. With $-X_1 = X_2 = X$, (5.18) is

$$\lambda_1^4 = \frac{2048}{\pi^3 G^2}\left(1 - \frac{b_2}{b_1}\right)\mathrm{e}^{-2X} = \frac{2048}{\pi^3 G^2}\left(1 - \frac{b_1}{b_2}\right)\mathrm{e}^{-2X}.$$

Thus $b_2^2 = b_1^2$ so that $b_2 = \pm b_1$. The additional solution $b_2 = -b_1$ has positive eigenvalue

$$\lambda = \frac{8\mathrm{e}^{-X/2}}{\pi^{3/4}} = \frac{2^{7/4}X^{1/4}}{\pi^{1/2}}G^{1/2}.$$

Three humps:. With $X_2 = 0$, $-X_1 = X_3 = X$, (5.18) is

$$\frac{\pi^3 G^2 \lambda_1^4}{2048} = \left(1 - \frac{b_2}{b_1}\right)\mathrm{e}^{-X} = \left(1 - \frac{b_3}{b_2}\right)\mathrm{e}^{-X} + \left(1 - \frac{b_1}{b_2}\right)\mathrm{e}^{-X} = \left(1 - \frac{b_2}{b_3}\right)\mathrm{e}^{-X},$$

with solution $(b_1, b_2, b_3) = (1, 1, 1)$ as expected along with the additional solutions

$$(b_1, b_2, b_3) = (1, -2, 1), \qquad (1, 0, -1),$$

which have corresponding positive eigenvalues

$$\lambda = \frac{2^{3/2}3^{1/4}X^{1/4}}{\pi^{1/2}}G^{1/2}, \qquad \lambda = \frac{2^{3/2}X^{1/4}}{\pi^{1/2}}G^{1/2}.$$

Four humps:. With $-X_1 = X_4 = Y_2$, $-X_2 = X_3 = Y_1$, in addition to $\mathbf{b} = (b_1, b_2, b_3, b_4) = (1, 1, 1, 1)$ the solutions of (5.18) are

$$\mathbf{b} = (-1, 1, 1, -1),$$
$$\mathbf{b} = \left(1 + r - (r^2 + 2r + 2)^{1/2}, 1, -1, -1 - r + (r^2 + 2r + 2)^{1/2}\right),$$
$$\mathbf{b} = \left(1 + r + (r^2 + 2r + 2)^{1/2}, 1, -1, -1 - r - (r^2 + 2r + 2)^{1/2}\right),$$

where $r = Y_1/Y_2$, with corresponding positive eigenvalues

$$\lambda = \frac{2^{7/4}Y_2^{1/4}}{\pi^{1/2}}G^{1/2},$$
$$\lambda = \frac{2^{3/2}}{\pi^{1/2}}\left(2Y_2 + Y_1 + \left(Y_1^2 + 2Y_1Y_2 + 2Y_2^2\right)^{1/2}\right)^{1/4}G^{1/2},$$
$$\lambda = \frac{2^{3/2}}{\pi^{1/2}}\left(2Y_2 + Y_1 - \left(Y_1^2 + 2Y_1Y_2 + 2Y_2^2\right)^{1/2}\right)^{1/4}G^{1/2}.$$

5.2. Perturbation of $f = V_0'$: eigenvalues of $O(G)$. Let us anticipate that $\lambda = O(G)$ and write $\lambda = G\lambda_1$. We will see that these eigenvalues are much more difficult to approximate, and that there is some subtlety in the calculation which is not immediately apparent. In order to motivate the rather detailed calculation which follows later, we first present a plausible analysis along the same lines as subsection 5.1, which will turn out to be incorrect.

641 **5.2.1. Inner expansion near the ith hump.** With $\xi = X_i + x$, we try an expansion near
642 the ith hump of the form

643 $$f = a_i \sum_{k=0}^{\infty} G^k f_k,$$

644 with $f_0 = \mathrm{d}V_0/\mathrm{d}x$. Here a_i is the amplitude of the eigenfunction near the ith hump (playing
645 the role of b_i in §5.1.1). We must determine a_i as part of the problem, which will happen when
646 we consider the interaction between humps in §5.2.2. In the end we will find a homogeneous
647 linear system (5.26) for the a_i, which will determine the eigenvalue λ_1, along with a_i as the
648 components of the corresponding eigenvector.
649 At $O(G)$ we have

650 $$\frac{\mathrm{d}^2 f_1}{\mathrm{d}x^2} + V_0^4(2f_1^* + 3f_1) - f_1 = -\mathrm{i}\lambda_1 \frac{\mathrm{d}V_0}{\mathrm{d}x}.$$

651 The solvability conditions are automatically satisfied, λ_1 is undetermined, and

652 $$f_1 = -\frac{\lambda_1 \mathrm{i}x}{2} V_0.$$

653 At $O(G^2)$

654 (5.19) $$\frac{\mathrm{d}^2 f_2}{\mathrm{d}x^2} + V_0^4(2f_2^* + 3f_2) - f_2 = -\frac{\lambda_1^2 x}{2} V_0 - \frac{(x+X_i)^2}{4}\frac{\mathrm{d}V_0}{\mathrm{d}x} - 20V_1V_0^3\frac{\mathrm{d}V_0}{\mathrm{d}x}.$$

655 The solvability condition (5.7) is not automatic, and will determine λ_1. We can simplify the
656 right-hand side of (5.7) using (4.11). Differentiating (4.11) gives

657 $$\frac{\mathrm{d}^3 V_1}{\mathrm{d}x^3} + 5V_0^4\frac{\mathrm{d}V_1}{\mathrm{d}x} + 20V_0^3V_1\frac{\mathrm{d}V_0}{\mathrm{d}x} - \frac{\mathrm{d}V_1}{\mathrm{d}x} = -\frac{(x+X_i)}{2}V_0 - \frac{(x+X_i)^2}{4}\frac{\mathrm{d}V_0}{\mathrm{d}x}.$$

658 Thus

659 $$\int_{-R}^{R}\left(\frac{(x+X_i)^2}{4}\frac{\mathrm{d}V_0}{\mathrm{d}x} + 20V_1V_0^3\frac{\mathrm{d}V_0}{\mathrm{d}x}\right)\frac{\mathrm{d}V_0}{\mathrm{d}x}\,\mathrm{d}x$$

660 $$= \int_{-R}^{R}\left(-\frac{(x+X_i)}{2}V_0 - \frac{\mathrm{d}^3V_1}{\mathrm{d}x^3} - 5V_0^4\frac{\mathrm{d}V_1}{\mathrm{d}x} + \frac{\mathrm{d}V_1}{\mathrm{d}x}\right)\frac{\mathrm{d}V_0}{\mathrm{d}x}\,\mathrm{d}x$$

661 $$= \int_{-R}^{R} -\frac{(x+X_i)}{2}V_0\frac{\mathrm{d}V_0}{\mathrm{d}x} - \left(\frac{\mathrm{d}^3V_0}{\mathrm{d}x^3} + 5V_0^4\frac{\mathrm{d}V_0}{\mathrm{d}x} - \frac{\mathrm{d}V_0}{\mathrm{d}x}\right)\frac{\mathrm{d}V_1}{\mathrm{d}x}\,\mathrm{d}x - \left[\frac{\mathrm{d}^2V_1}{\mathrm{d}x^2}\frac{\mathrm{d}V_0}{\mathrm{d}x} - \frac{\mathrm{d}V_1}{\mathrm{d}x}\frac{\mathrm{d}^2V_0}{\mathrm{d}x^2}\right]_{-R}^{R}$$

662 $$= \int_{-R}^{R}\frac{1}{4}V_0^2\,\mathrm{d}x - \left[\frac{\mathrm{d}^2V_1}{\mathrm{d}x^2}\frac{\mathrm{d}V_0}{\mathrm{d}x} - \frac{\mathrm{d}V_1}{\mathrm{d}x}\frac{\mathrm{d}^2V_0}{\mathrm{d}x^2}\right]_{-R}^{R}.$$

663 Thus the solvability conditions on (5.19) may be written

664 (5.20) $$\mathrm{Im}\left[\frac{\mathrm{d}f_2}{\mathrm{d}x}V_0 - f_2\frac{\mathrm{d}V_0}{\mathrm{d}x}\right]_{-R}^{R} = 0,$$

665 $$\mathrm{Re}\left[\frac{\mathrm{d}f_2}{\mathrm{d}x}\frac{\mathrm{d}V_0}{\mathrm{d}x} - f_2\frac{\mathrm{d}^2V_0}{\mathrm{d}x^2}\right]_{-R}^{R} = \frac{(\lambda_1^2-1)}{4}\int_{-R}^{R}V_0^2\,\mathrm{d}x + \left[\frac{\mathrm{d}^2V_1}{\mathrm{d}x^2}\frac{\mathrm{d}V_0}{\mathrm{d}x} - \frac{\mathrm{d}V_1}{\mathrm{d}x}\frac{\mathrm{d}^2V_0}{\mathrm{d}x^2}\right]_{-R}^{R}.$$

666 To evaluate the left-hand side we need to consider the region between the humps.

5.2.2. In between the humps. As usual consider the gap between X_i and X_{i+1}. In this region

$$\mathrm{i}G\lambda_1 f + \frac{\mathrm{d}^2 f}{\mathrm{d}\xi^2} - f + \frac{G^2\xi^2}{4} f = O(fG^8 \log^4 G). \tag{5.21}$$

Expanding

$$f = \sum_{k=0}^{\infty} G^k f_k,$$

gives

$$\frac{\mathrm{d}^2 f_0}{\mathrm{d}\xi^2} - f_0 = 0, \tag{5.22}$$

at leading order. Matching requires

$$f \sim 12^{1/4} a_{i+1} \mathrm{e}^{\xi - X_{i+1}} \quad \text{as } \xi \to X_{i+1}, \qquad f \sim -12^{1/4} a_i \mathrm{e}^{-\xi + X_i} \quad \text{as } \xi \to X_i.$$

Thus

$$f_0 = 12^{1/4} a_{i+1} \mathrm{e}^{\xi - X_{i+1}} - 12^{1/4} a_i \mathrm{e}^{-\xi + X_i}.$$

In terms of $\xi = X_{i+1} + x$ this is

$$f_0 = 12^{1/4} a_{i+1} \mathrm{e}^{x} - 12^{1/4} a_i \mathrm{e}^{-x + X_i - X_{i+1}}.$$

Since $\mathrm{e}^{X_i - X_{i+1}} = O(G^2)$ the additional term matches with $G^2 f_2$ from the $(i+1)$th hump, giving the matching condition

$$a_{i+1} f_2 G^2 \sim -12^{1/4} a_i \mathrm{e}^{-x + X_i - X_{i+1}},$$

as $x \to -\infty$ for the near-hump solution. In terms of $\xi = X_i + x$ the between-hump solution is

$$f_0 = 12^{1/4} a_{i+1} \mathrm{e}^{x + X_i - X_{i+1}} - 12^{1/4} a_i \mathrm{e}^{-x},$$

giving the matching condition

$$a_i f_2 G^2 \sim 12^{1/4} a_{i+1} \mathrm{e}^{x + X_i - X_{i+1}},$$

as $x \to \infty$ for the near-hump solution. Thus

$$\lim_{R\to\infty} \operatorname{Im} \left[\frac{\mathrm{d}f_2}{\mathrm{d}x} V_0 - f_2 \frac{\mathrm{d}V_0}{\mathrm{d}x} \right]_{-R}^{R} = 0, \tag{5.23}$$

$$\lim_{R\to\infty} \operatorname{Re} \left[a_i \frac{\mathrm{d}f_2}{\mathrm{d}x} \frac{\mathrm{d}V_0}{\mathrm{d}x} - a_i f_2 \frac{\mathrm{d}^2 V_0}{\mathrm{d}x^2} \right]_{-R}^{R} = -4\sqrt{3} a_{i+1} \frac{\mathrm{e}^{-X_{i+1} + X_i}}{G^2} - 4\sqrt{3} a_{i-1} \frac{\mathrm{e}^{-X_i + X_{i-1}}}{G^2}, \tag{5.24}$$

$$\lim_{R\to\infty} \left[\frac{\mathrm{d}^2 V_1}{\mathrm{d}x^2} \frac{\mathrm{d}V_0}{\mathrm{d}x} - \frac{\mathrm{d}V_1}{\mathrm{d}x} \frac{\mathrm{d}^2 V_0}{\mathrm{d}x^2} \right]_{-R}^{R} = -4\sqrt{3} \frac{\mathrm{e}^{-X_{i+1} + X_i}}{G^2} - 4\sqrt{3} \frac{\mathrm{e}^{-X_i + X_{i-1}}}{G^2}. \tag{5.25}$$

5.2.3. Solvability condition. Letting $R \to \infty$, the solvability condition (5.20) is satisfied, and, noting that

$$\int_{-\infty}^{\infty} V_0^2 \, \mathrm{d}x = \frac{\sqrt{3}\,\pi}{2},$$

subsection 5.2.1 becomes

$$(\lambda_1^2 - 1)\frac{\pi}{32} a_i = (a_i - a_{i+1})\frac{\mathrm{e}^{X_i - X_{i+1}}}{G^2} + (a_i - a_{i-1})\frac{\mathrm{e}^{X_{i-1} - X_i}}{G^2}, \qquad i = 1, \ldots, n. \tag{5.26}$$

Equation (5.26) are a homogeneous set of linear equations for a_i, $i = 1, \ldots, n$. For a non-trivial solution the determinant must vanish, which determines the eigenvalue λ_1: $(\lambda_1^2 - 1)\pi/32$ is an eigenvalue of this system, with a_i the components of the corresponding eigenvector. Note that $\lambda_1 = \pm 1$, $a_i = a$ for all i, is always a solution, corresponding to a global translation. Note also that the eigenvalues again come in pairs—for every positive eigenvalue there is a negative eigenvalue of equal modulus.

5.2.4. Examples.

Two humps. With $-X_1 = X_2 = X$ equation (5.26) gives

$$\lambda_1^2 = 1 + \left(1 - \frac{a_2}{a_1}\right) X = 1 + \left(1 - \frac{a_1}{a_2}\right) X.$$

Thus $a_1 = \pm a_2$, and it appears there are solutions

$$(a_1, a_2) = (1, 1), \qquad (a_1, a_2) = (-1, 1),$$

with corresponding positive eigenvalues

$$\lambda = G, \qquad \lambda = (1 + 2X)^{1/2} G.$$

Three humps. For the three-bump case with $-X_1 = X_3 = X$, $X_2 = 0$, (5.26) gives

$$\lambda_1^2 = 1 + \left(1 - \frac{a_2}{a_1}\right) X = 1 + \left(1 - \frac{a_3}{a_2}\right) X + \left(1 - \frac{a_1}{a_2}\right) X = 1 + \left(1 - \frac{a_2}{a_3}\right) X.$$

Writing $(a_1, a_2, a_3) = \mathbf{a}$ the solutions are

$$\mathbf{a} = (1, 1, 1), \qquad \mathbf{a} = (1, 0, -1) \qquad \text{and} \qquad \mathbf{a} = (1, -2, 1),$$

with corresponding positive eigenvalues

$$\lambda = G, \qquad \lambda = (1 + X)^{1/2} G, \qquad \lambda = (1 + 3X)^{1/2} G. \tag{5.27}$$

Four humps. With $-X_1 = X_4 = Y_2$, $-X_2 = X_3 = Y_1$, equation (5.26) gives

$$\begin{aligned} \lambda_1^2 &= 1 + \left(1 - \frac{a_2}{a_1}\right) Y_2 = 1 + \left(1 - \frac{a_3}{a_2}\right)(Y_1 + Y_2) + \left(1 - \frac{a_1}{a_2}\right) Y_2 \\ &= 1 + \left(1 - \frac{a_4}{a_3}\right) Y_2 + \left(1 - \frac{a_2}{a_3}\right)(Y_1 + Y_2) = 1 + \left(1 - \frac{a_3}{a_4}\right) Y_2. \end{aligned}$$

With $\mathbf{a} = (a_1, a_2, a_3, a_4)$, there are solutions

$$\mathbf{a} = (1, 1, 1, 1),$$
$$\mathbf{a} = (-1, 1, 1, -1),$$
$$\mathbf{a} = \left(1 + r - (r^2 + 2r + 2)^{1/2}, 1, -1, -1 - r + (r^2 + 2r + 2)^{1/2}\right),$$
$$\mathbf{a} = \left(1 + r + (r^2 + 2r + 2)^{1/2}, 1, -1, -1 - r - (r^2 + 2r + 2)^{1/2}\right),$$

where $r = Y_1/Y_2$, with corresponding positive eigenvalues

$$\lambda = G,$$
$$\lambda = (1 + 2Y_2)^{1/2} G,$$
$$\lambda = \left(1 + 2Y_2 + Y_1 + \left(Y_1^2 + 2Y_1Y_2 + 2Y_2^2\right)^{1/2}\right)^{1/2} G,$$
$$\lambda = \left(1 + 2Y_2 + Y_1 - \left(Y_1^2 + 2Y_1Y_2 + 2Y_2^2\right)^{1/2}\right)^{1/2} G.$$

In Figure 11 we show a comparison between the predictions of (5.26) and our numerical solutions.

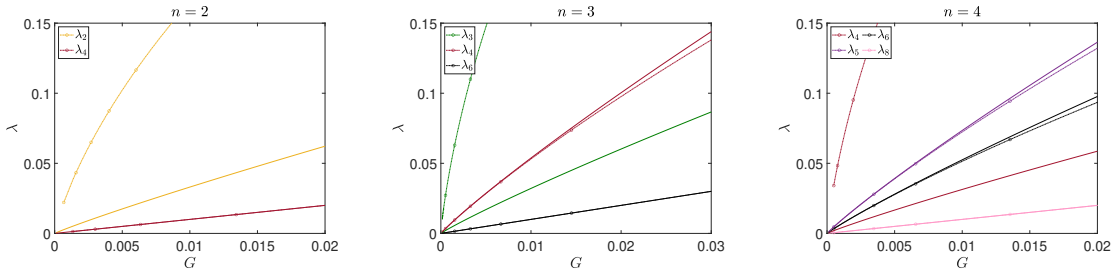

(a) (b) (c)

Figure 11: Comparison of the eigenvalues proportional to G. The solid lines are the asymptotic predictions of (5.26); the lines with circles correspond to the numerically calculated values.

We see that some of the eigenvalues are well approximated, but in each case there is a large eigenvalue that the asymptotic prediction misses, and there is a predicted eigenvalue which is not present numerically. To understand why this is the case we have to return to our assumptions about the form of the eigenfunctions.

5.3. Why the naive asymptotic solution fails. Having determined that both $\mathrm{i}V_0$ and $\mathrm{d}V_0/\mathrm{d}x$ satisfy the leading-order problem when λ is small, we should really consider a leading order solution in the near-hump region of the form

$$f_0 = a_i \frac{\mathrm{d}V_0}{\mathrm{d}x} + b_i \mathrm{i}V_0, \tag{5.28}$$

i.e., we should combine both solutions rather than considering them separately. For the single-hump solution these eigenfunctions can be considered independently, but for the multi-hump

solutions they interact with each other. Let us suppose that $\lambda = \lambda_1 G$ and proceed using (5.28) as the first term in the expansion near the ith hump. Then we would find that there are solvability conditions at $O(G^2)$, which are of the form

$$\begin{bmatrix} A(\lambda_1) & 0 \\ 0 & B \end{bmatrix} \begin{bmatrix} \mathbf{a} \\ \mathbf{b} \end{bmatrix} = \begin{bmatrix} \mathbf{0} \\ \mathbf{0} \end{bmatrix},$$

where $\mathbf{a}$ and $\mathbf{b}$ are vectors with components a_i and b_i respectively, A is the matrix representing the linear (5.26), and B is the matrix representing the linear (5.18) but with λ_1 set to zero, i.e.

$$(b_i - b_{i+1}) \frac{e^{X_i - X_{i+1}}}{G^2} + (b_i - b_{i-1}) \frac{e^{X_{i-1} - X_i}}{G^2} = 0. \tag{5.29}$$

In our analysis in subsection 5.2 we set $\det(A) = 0$ to determine the eigenvalue λ_1, and assumed that $\mathbf{b} = \mathbf{0}$. However, as we observed when writing down (5.18), the matrix B is singular, with null vector $(1, 1, \ldots, 1)$. Thus there is still a degree of freedom which is undetermined at this order, which will be determined at the next order in the expansions. This means that we can no longer ignore the fact that $\mathbf{a}$, $\mathbf{b}$ and λ should also be expanded in powers of G.

If we do so, following the scheme above, then we find that the leading-order solvability condition is

$$\begin{bmatrix} A(\lambda_1) & 0 \\ 0 & B \end{bmatrix} \begin{bmatrix} \mathbf{a}^{(0)} \\ \mathbf{b}^{(0)} \end{bmatrix} = \begin{bmatrix} \mathbf{0} \\ \mathbf{0} \end{bmatrix},$$

so that λ_1 is an eigenvalue of A, with $\mathbf{a}^{(0)}$ the corresponding normalised eigenvector, and $\mathbf{b}^{(0)} = b^{(0)}(1, 1, \ldots, 1)$ with $b^{(0)}$ still undetermined. Proceeding with the expansion we would find solvability conditions at the next order of the form

$$\begin{bmatrix} A(\lambda_1) & 0 \\ 0 & B \end{bmatrix} \begin{bmatrix} \mathbf{a}^{(1)} \\ \mathbf{b}^{(1)} \end{bmatrix} = \begin{bmatrix} \lambda_2 C_1 \mathbf{a}^{(0)} + C_2 \mathbf{b}^{(0)} \\ C_3 \mathbf{a}^{(0)} \end{bmatrix}, \tag{5.30}$$

for some matrices C_1, C_2, C_3. Note in particular that terms involving $\mathbf{b}^{(0)}$ appear on the right-hand side of the equation for $\mathbf{a}^{(1)}$ while terms involving $\mathbf{a}^{(0)}$ appear on the right-hand side of the equation for $\mathbf{b}^{(1)}$. Now both the matrix $A(\lambda_1)$ and the matrix B are singular, so there are solvability conditions on the two right-hand sides. But both the degrees of freedom we have—λ_2 and $b^{(0)}$—appear on the RHS of the equation for $\mathbf{a}^{(1)}$. The solvability condition for $B\mathbf{b}^{(1)} = C_3 \mathbf{a}^{(0)}$ may or may not be satisfied; we have no parameter in the equation to adjust to ensure that it is. This explains why the naive asymptotic approximation in subsection 5.2 predicted solutions which were not found numerically—if we had continued to the next order in the expansion we would have found a solvability condition that we could not satisfy.

In order to solve the problem of both remaining degrees of freedom appearing in the same block of (5.30) we need to make $\mathbf{b}$ an order of G larger than $\mathbf{a}$. Suppose, therefore, that $\mathbf{a}^{(0)} = \mathbf{0}$. Then the leading-order solvability conditions give

$$B\mathbf{b}^{(0)} = \mathbf{0}, \tag{5.31}$$

so that $\mathbf{b}^{(0)} = b^{(0)}(1, 1, \ldots, 1)$. At next order we will find

$$\begin{bmatrix} A(\lambda_1) & 0 \\ 0 & B \end{bmatrix} \begin{bmatrix} \mathbf{a}^{(1)} \\ \mathbf{b}^{(1)} \end{bmatrix} = \begin{bmatrix} C_2\mathbf{b}^{(0)} \\ 0 \end{bmatrix}. \tag{5.32}$$

Since $\mathbf{b}^{(0)}$ is non-zero there is a non-trivial solution $\mathbf{a}^{(1)} = A^{-1}C_2\mathbf{b}^{(0)}$ when A is non-singular. Thus λ_1 is still undetermined, but the relative scaling of $\mathbf{a}^{(1)}$ and $\mathbf{b}^{(0)}$ is determined. Now, at next order, we will find

$$\begin{bmatrix} A(\lambda_1) & 0 \\ 0 & B \end{bmatrix} \begin{bmatrix} \mathbf{a}^{(2)} \\ \mathbf{b}^{(2)} \end{bmatrix} = \begin{bmatrix} \lambda_2 C_1\mathbf{a}^{(1)} + C_2\mathbf{b}^{(1)} \\ C_3\mathbf{a}^{(1)} + C_4\mathbf{b}^{(0)} \end{bmatrix}. \tag{5.33}$$

Crucially, since $\mathbf{a}^{(0)}$ is a function of λ_1, the solvability condition on the second block can be satisfied and determines the eigenvalue λ_1. Now that we know schematically the structure of the expansions, let us work through some of the details.

5.4. More careful analysis of the eigenvalues $\lambda = O(G)$. We suppose that

$$\lambda = \sum_{k=1}^{\infty} \lambda_k G^k. \tag{5.34}$$

Near the i th hump, with $\xi = X_i + x$, we set

$$f = a_i U + b_i W, \tag{5.35}$$

where

$$f = \sum_{k=0}^{\infty} G^k f_k, \qquad U = \sum_{k=0}^{\infty} G^k U_k, \qquad W = \sum_{k=0}^{\infty} G^k W_k, \tag{5.36}$$

with

$$U_0 = \frac{\mathrm{d}V_0}{\mathrm{d}x}, \qquad W_0 = \mathrm{i}V_0. \tag{5.37}$$

We also expand a_i and b_i in powers of G, anticipating the interleaving expansions,

$$a_i = Ga_i^{(1)} + G^3 a_i^{(3)} + \cdots, \qquad b_i = b_i^{(0)} + G^2 b_i^{(2)} + \cdots. \tag{5.38}$$

Since the analysis gets now very technical, and we need to match many orders of inner and outer expansions, we defer many of the details to the Supplementary Material, and here simply pick out some of the key equations. At $O(G^2)$ in the inner expansion near the i th hump we find the solvability condition (SM4.8),

$$b_i^{(0)} \left(\frac{4\sqrt{3}}{G^2} \mathrm{e}^{-X_{i+1}+X_i} + \frac{4\sqrt{3}}{G^2} \mathrm{e}^{-X_i+X_{i-1}} \right) = \frac{4\sqrt{3}\, b_{i+1}^{(0)}}{G^2} \mathrm{e}^{X_i - X_{i+1}} + \frac{4\sqrt{3}\, b_{i-1}^{(0)}}{G^2} \mathrm{e}^{X_{i-1} - X_i}. \tag{5.39}$$

As anticipated, this is (5.18) with λ_1 set to zero, and is equation (5.31), $B\mathbf{b}^{(0)} = \mathbf{0}$, from subsection 5.3. Equation (5.39)) fixes $b_i^{(0)} = b^{(0)}$ for all i.

At $O(G^3)$ in the inner expansion near the ith hump we find the solvability condition (SM4.22),

$$\frac{\pi a_i^{(1)}(\lambda_1^2-1)}{32} + (a_{i+1}^{(1)} - a_i^{(1)})\frac{\mathrm{e}^{X_i - X_{i+1}}}{G^2} + (a_{i-1}^{(1)} - a_i^{(1)})\frac{\mathrm{e}^{-X_i + X_{i-1}}}{G^2} = \frac{3\pi}{64}\lambda_1 b^{(0)} X_i - \frac{\lambda_1 b^{(0)}}{2}(X_i - X_{i+1})\frac{\mathrm{e}^{X_i - X_{i+1}}}{G^2} - \frac{\lambda_1 b^{(0)}}{2}(X_i - X_{i-1})\frac{\mathrm{e}^{-X_i + X_{i-1}}}{G^2}. \tag{5.40}$$

Equation (5.40) is (5.32), $A(\lambda_1)\mathbf{a}^{(1)} = C_2\mathbf{b}^{(0)}$, from subsection 5.3. When $b^{(0)}$ is non-zero it gives $a_i^{(1)}$ in terms of $b^{(0)}$, with no restriction on λ_1. To determine λ_1 we need to go to one more order. Note that there is still the possibility that $b^{(0)} = 0$, in which case λ_1 is determined by $\det A = 0$ and $\mathbf{a}^{(1)}$ is a null vector of A.

At $O(G^4)$ in the inner expansion near the ith hump we find the solvability condition (SM4.29),

$$\begin{aligned}&\frac{b^{(0)}\lambda_1^2(\lambda_1^2-4)\pi^3}{512} + \frac{3\pi\lambda_1 X_i}{64}(b^{(0)}\lambda_1 X_i - 2a_i^{(1)}) + 4(b_{i+1}^{(2)} - b_i^{(2)})\frac{\mathrm{e}^{X_i - X_{i+1}}}{G^2} \\ &+ 4(b_{i-1}^{(2)} - b_i^{(2)})\frac{\mathrm{e}^{X_{i-1} - X_i}}{G^2} + 2a_{i+1}^{(1)}(X_{i+1} - X_i)\lambda_1\frac{\mathrm{e}^{X_i - X_{i+1}}}{G^2} + 2a_{i-1}^{(1)}(X_{i-1} - X_i)\lambda_1\frac{\mathrm{e}^{X_{i-1} - X_i}}{G^2} \\ &- 3a_{i+1}^{(1)}\lambda_1\frac{\mathrm{e}^{X_i - X_{i+1}}}{G^2} + 3a_{i-1}^{(1)}\lambda_1\frac{\mathrm{e}^{X_{i-1} - X_i}}{G^2} + \frac{\lambda_1^2}{2}b^{(0)}\frac{\mathrm{e}^{X_i - X_{i+1}}}{G^2}\left(-X_i^2 + 3X_{i+1} + 2X_iX_{i+1} - X_{i+1}^2\right) \\ &+ \frac{\lambda_1^2}{2}b^{(0)}\frac{\mathrm{e}^{X_{i-1} - X_i}}{G^2}\left(-X_i^2 - 3X_{i-1} + 2X_iX_{i-1} - X_{i-1}^2\right) = 0.\end{aligned} \tag{5.41}$$

This is (5.33), $B\mathbf{b}^{(2)} = C_3\mathbf{a}^{(1)} + C_4\mathbf{b}^{(0)}$, from subsection 5.3. Since B has the null vector $(1, 1, \ldots, 1)$ these equations for $b_i^{(2)}$ have a solvability condition: if we sum over i then $b_i^{(2)}$ vanishes. This sum over i is the equation which determines λ_1.

Let us first identify which of the eigenvalues of subsection 5.2 survive the new solvability condition (5.41).

5.4.1. Eigenvalues which follow the old scheme of subsection 5.2. We found some numerically determined eigenvalues did match the predictions of subsection 5.2. If $b^{(0)} = 0$ then the eigenvalue is determined by requiring a non-trivial solution of (5.40),

$$\frac{\pi a_i^{(1)}(\lambda_1^2-1)}{32} + (a_{i+1}^{(1)} - a_i^{(1)})\frac{\mathrm{e}^{X_i - X_{i+1}}}{G^2} + (a_{i-1}^{(1)} - a_i^{(1)})\frac{\mathrm{e}^{-X_i + X_{i-1}}}{G^2} = 0, \tag{5.42}$$

as in subsection 5.2, but the extra solvability condition given by (5.41) must also be satisfied, which is

$$\begin{aligned}&\sum_{i=1}^{n} -\frac{3\pi\lambda_1 X_i}{32}a_i^{(1)} + 2a_{i+1}^{(1)}(X_{i+1} - X_i)\lambda_1\frac{\mathrm{e}^{X_i - X_{i+1}}}{G^2} \\ &+ 2a_{i-1}^{(1)}(X_{i-1} - X_i)\lambda_1\frac{\mathrm{e}^{X_{i-1} - X_i}}{G^2} - 3a_{i+1}^{(1)}\lambda_1\frac{\mathrm{e}^{X_i - X_{i+1}}}{G^2} + 3a_{i-1}^{(1)}\lambda_1\frac{\mathrm{e}^{X_{i-1} - X_i}}{G^2} = 0.\end{aligned} \tag{5.43}$$

In general we would not expect this to be satisfied, but certain symmetries of the $a_i^{(1)}$ may mean it is satisfied automatically. In particular, with some index relabelling, (5.43) is

$$\sum_{i=1}^{n} -\frac{3\pi X_i}{32}a_i^{(1)} + 2(a_i^{(1)} - a_{i-1}^{(1)})X_i\frac{\mathrm{e}^{X_{i-1}-X_i}}{G^2} + 2(a_i^{(1)} - a_{i+1}^{(1)})X_i\frac{\mathrm{e}^{X_i-X_{i+1}}}{G^2} - 3a_i^{(1)}\frac{\mathrm{e}^{X_{i-1}-X_i}}{G^2} + 3a_i^{(1)}\frac{\mathrm{e}^{X_i-X_{i+1}}}{G^2} = 0.$$

Simplifying using (5.42) and (4.15) gives

$$\sum_{i=1}^{n} -3X_i a_i^{(1)} + (\lambda_1^2 - 1)a_i^{(1)} = 0. \tag{5.44}$$

Since, by symmetry, $\sum_{i=1}^{n} X_i = 0$ we find the eigenvalue $\lambda_1 = \pm 1$ with eigenvector $a_i^{(1)} = 1$ for $i = 1, \ldots, n$ always works as it should.

Two humps. With $-X_1 = X_2 = X$ we found

$$\mathbf{a} = (-1, 1), \qquad \mathbf{a} = (1, 1),$$

with corresponding positive eigenvalues

$$\lambda = (1 + 2X)^{1/2}G, \qquad \lambda = G.$$

The second satisfies (5.44) but the first does not, in agreement with Figure 11(a).

Three humps. For the three-bump case with $-X_1 = X_3 = X$, $X_2 = 0$, we found

$$\mathbf{a} = (1, -2, 1), \qquad \mathbf{a} = (1, 0, -1) \qquad \text{and} \qquad \mathbf{a} = (1, 1, 1),$$

with corresponding positive eigenvalues

$$\lambda = (1 + 3X)^{1/2}G, \qquad \lambda = (1 + X)^{1/2}G, \qquad \lambda = G. \tag{5.45}$$

The first and third satisfy (5.44), but the second does not, in agreement with Figure 11(b).

Four humps. With $-X_1 = X_4 = Y_2$, $-X_2 = X_3 = Y_1$, we found

$$\mathbf{a} = \left(1 + r - (r^2 + 2r + 2)^{1/2}, 1, -1, -1 - r + (r^2 + 2r + 2)^{1/2}\right),$$
$$\mathbf{a} = (-1, 1, 1, -1),$$
$$\mathbf{a} = \left(1 + r + (r^2 + 2r + 2)^{1/2}, 1, -1, -1 - r - (r^2 + 2r + 2)^{1/2}\right),$$
$$\mathbf{a} = (1, 1, 1, 1),$$

where $r = Y_1/Y_2$, with corresponding positive eigenvalues

$$\lambda = \left(1 + 2Y_2 + Y_1 + \left(Y_1^2 + 2Y_1Y_2 + 2Y_2^2\right)^{1/2}\right)^{1/2} G,$$
$$\lambda = (1 + 2Y_2)^{1/2}G,$$
$$\lambda = \left(1 + 2Y_2 + Y_1 - \left(Y_1^2 + 2Y_1Y_2 + 2Y_2^2\right)^{1/2}\right)^{1/2} G,$$
$$\lambda = G.$$

The second and fourth satisfy (5.44), but the first and third do not. It appears in Figure 11(c) that we correctly predicted the first eigenvalue also. However, this was merely a coincidence, and the first eigenfunction in fact follows the new scheme with nonzero $b^{(0)}$.

5.4.2. Eigenvalues which follow the new scheme.

Two humps. With $-X_1 = X_2 = X$ the sum over i of (SM4.29) is

$$\frac{\lambda_1^2(\lambda_1^2-4)\pi(\pi^2(\lambda_1^2-1-2X)+8X^2(3-4X))}{256(\lambda_1^2-1-2X)} = 0. \tag{5.46}$$

We see the positive eigenvalue $\lambda_1 = 2$, and also a singularity at the false eigenvalue $\lambda_1 = (1+2X)^{1/2}$ of subsection 5.2. There is one other positive eigenvalue given by

$$\lambda_1 = \left(1 + 2X + \frac{8X^2(4X-3)}{\pi^2}\right)^{1/2}. \tag{5.47}$$

The corresponding eigenvector is

$$\mathbf{b}^{(0)} = (1,1), \qquad \mathbf{a}^{(1)} = \frac{\lambda_1 X(2X-3)}{2(\lambda_1^2-1-2X)}(1,-1).$$

Thus, together, the correct eigenvalues of $O(G)$ are

$$\lambda \sim G, \qquad \lambda \sim 2G, \qquad \lambda \sim G\left(1 + 2X + \frac{8X^2(4X-3)}{\pi^2}\right)^{1/2}.$$

A comparison with numerical computations is shown in Fig. 7(a).

Three humps. With $-X_1 = X_3 = X$, $X_2 = 0$, the sum over i of (SM4.29) is

$$\frac{\lambda_1^2(\lambda_1^2-4)\pi(3\pi^2(\lambda_1^2-1-X)+16X^2(3-2X))}{512(\lambda_1^2-1-X)} = 0. \tag{5.48}$$

We see the positive eigenvalue $\lambda_1 = 2$, and also a singularity at the false eigenvalue $\lambda_1 = (1+X)^{1/2}$ of subsection 5.2. There is one other positive eigenvalue given by

$$\lambda_1 = \left(1 + X + \frac{16X^2(2X-3)}{3\pi^2}\right)^{1/2}. \tag{5.49}$$

The corresponding eigenvector is

$$\mathbf{b}^{(0)} = (1,1,1), \qquad \mathbf{a}^{(1)} = \frac{\lambda_1 X(X-3)}{2(\lambda_1^2-1-X)}(1,0,-1).$$

Thus, together, the correct eigenvalues of $O(G)$ are

$$\lambda \sim G, \qquad \lambda \sim (1+3X)^{1/2}G, \qquad \lambda \sim 2G, \qquad \lambda \sim G\left(1 + X + \frac{16X^2(2X-3)}{3\pi^2}\right)^{1/2}.$$

A comparison with numerical computations is shown in Fig. 7(b).

Four humps. With $-X_1 = X_4 = Y_2$, $-X_2 = X_3 = Y_1$, the sum over i of (SM4.29) has two positive solutions in addition to $\lambda_1 = 2$. These, together with

$$\lambda \sim G, \qquad \lambda \sim (1 + 2Y_2)^{1/2} G,$$

are the correct eigenvalues of $O(G)$. A comparison with numerical computations is shown in Fig. 7(c).

6. Conclusions and Future Challenges. In the present work we have revisited the topic of multi-pulse collapsing solutions in the context of the one-dimensional nonlinear Schrödinger equation with a power-law nonlinearity. Returning to the results of [9] from a novel perspective, we have showcased not only in a qualitative, but also in a quantitative way, how *countably infinitely many* branches of such solutions bifurcate from the critical point, along with their most well-known cousin, namely the stationary single collapse point waveform. We have shown that all of these solutions emerge from an infinite distance between the pulses in an example of "bifurcation from infinity" with the distance between the pulses shrinking as the growth rate of the collapse increases. We have provided quantitative characterizations both for the bifurcation curve of the relevant waveforms for the blowup rate G as a function of σ, as well as for the separation between their peaks as a function of G. Importantly, we have also tackled both qualitatively and quantitatively the spectral stability analysis of the relevant states. Indeed, we have found all of them to be unstable, bearing $n-1$ pairs of eigenvalues of size approximately $G^{1/2}$, another $n+1$ pairs of size practically proportional to G, while $n-1$ pairs emerge on the imaginary axis, and one remains in the vicinity of the origin. We have verified the relevant count for cases of $n = 1$ to $n = 4$ and indeed examined cases even up to $n = 6$. While some of the $\mathrm{O}(G^{1/2})$ eigenvalues were less accurately captured when G was large, generally our predictions were found to be in excellent qualitative and good quantitative agreement with the numerical observations. Finally, some select dynamical simulations gave us the opportunity to observe the symmetry breaking events leading to the instability of the multi-pulse configurations and the eventual predominance of a single pulse, in line with the expectations associated with stability based on our eigenvector analysis.

Naturally, this study paves the way for a number of directions of future study. Arguably, the most canonical of these concerns whether such multi-bump collapsing solutions can be systematically found in higher dimensions. Our preliminary considerations along this vein suggest the existence of a wide range of possible higher-dimensional waveforms. For instance, in Figure 12, we illustrate a prototypical star-shaped self-similar waveform computed in the rescaled $(\xi, \eta) \equiv (x/L, y/L)$ space for the 2D NLS equation. Generalizations of the analytical considerations herein enable the consideration of multiple collapse "spots" as an intriguing interacting particle system in the higher-dimensional setting meriting investigation (in terms of its equilibria) in its own right. These can then potentially be associated with the recent experiments of [7] and offer a systematic explanation for the observations therein. These can also potentially be connected to the stability analysis of the *ring type solutions* that have been discovered in the work of [17, 8]. It would be particularly interesting to explore the spectral stability of the ring in terms of its eigenvalues in the co-exploding frame and the conditions under which these may potentially give rise to multi-pulse configurations as the parameters of the system (such as the nonlinearity exponent) may vary. From a computational perspective,

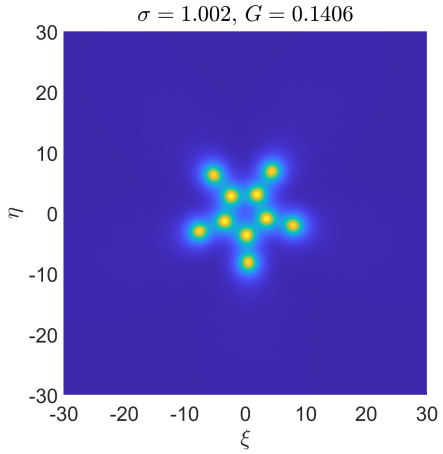

Figure 12: Star-shaped self-similar profile, $|v(\xi, \eta)|$, for the 2D NLS equation. Here, $\sigma = 1.002$ and the computed blow-up rate is $G = 0.1406$.

and especially for such higher- dimensional PDEs, domain decomposition methods [15, 37] together with the parallelization features provided by the Portable, Extensible Toolkit for Scientific Computation (PETSc) [6] already embedded in FreeFEM [33] (and references therein) have provided us with the necessary computational environment to efficiently and reliably study these types of problems.

It is also relevant to point out here that recent experimental developments in optics have enabled the realization of fractional derivatives (in the form of derivatives of the Riesz type) which, in turn, allow for the manipulation of dispersion [22]. Considering the fractional Laplacian operator $(-\Delta)^{\alpha/2}$, with the Lévy index $0 < \alpha < 2$, this experimental realization has made considerations in the vicinity of $\alpha = 1$ possible. This constitutes (even for the cubic nonlinearity) a critical point for transition to collapse-type solutions and hence represents an additional area of possible future research for the waveforms and phenomena identified herein. Such studies are currently underway and the reporting of associated findings is deferred to future publications.

Acknowledgements. This work has been supported by the U.S. National Science Foundation under Grants DMS-2204782 (EGC), and PHY-2110030, PHY-2408988 and DMS-2204702 (PGK), and by the US National Science Foundation (IGK). EGC expresses his gratitude to Prof. Hannes Uecker (University of Oldenburg) for fruitful discussions related to the finite-element implementation of phase conditions in `pde2path` [38]. Also, EGC thanks Profs. Christopher Douglas (Duke), Pierre Jolivet (Sorbonne Université), Georges Sadaka (University of Rouen Normandie) for their continuing support and encouragement on technical aspects on `FreeFEM`.

REFERENCES

[1] M. Ablowitz, *Nonlinear Dispersive Waves, Asymptotic Analysis and Solitons*, Cambridge University

Press, Cambridge, 2011, https://doi.org/10.1017/cbo9780511998324.
[2] M. Ablowitz, B. Prinari, and A. Trubatch, *Discrete and Continuous Nonlinear Schrödinger Systems*, Cambridge University Press, Cambridge, 2004.
[3] M. J. Ablowitz and H. Segur, *Solitons and the inverse scattering transform*, SIAM, 1981.
[4] P. Amodio, C. J. Budd, O. Koch, V. Rottschäfer, G. Settanni, and E. Weinmüller, *Near critical, self-similar, blow-up solutions of the generalised korteweg–de vries equation: Asymptotics and computations*, Physica D: Nonlinear Phenomena, 401 (2020), p. 132179, https://doi.org/https://doi.org/10.1016/j.physd.2019.132179, https://www.sciencedirect.com/science/article/pii/S0167278918306018.
[5] B. Bakkali-Hassani, C. Maury, Y.-Q. Zou, E. Le Cerf, R. Saint-Jalm, P. C. M. Castilho, S. Nascimbene, J. Dalibard, and J. Beugnon, *Realization of a townes soliton in a two-component planar bose gas*, Phys. Rev. Lett., 127 (2021), p. 023603, https://doi.org/10.1103/PhysRevLett.127.023603, https://link.aps.org/doi/10.1103/PhysRevLett.127.023603.
[6] S. Balay and et. al., *PETSc/TAO Users Manual*, Argonne National Laboratory-21/39, https://petsc.org/release/docs/manual/manual.pdf, 2022.
[7] S. Banerjee, K. Zhou, S. K. Tiwari, H. Tamura, R. Li, P. Kevrekidis, S. I. Mistakidis, V. Walther, and C.-L. Hung, *Collapse of a quantum vortex in an attractive two-dimensional bose gas*, 2024, https://arxiv.org/abs/2406.00863.
[8] G. Baruch, G. Fibich, and N. Gavish, *Singular standing-ring solutions of nonlinear partial differential equations*, Physica D: Nonlinear Phenomena, 239 (2010), pp. 1968–1983, https://doi.org/https://doi.org/10.1016/j.physd.2010.07.009, https://www.sciencedirect.com/science/article/pii/S0167278910002198.
[9] C. J. Budd, S. Chen, and R. D. Russell, *New self-similar solutions of the nonlinear schrödinger equation with moving mesh computations*, Journal of Computational Physics, 152 (1999), pp. 756–789, https://doi.org/https://doi.org/10.1006/jcph.1999.6262, https://www.sciencedirect.com/science/article/pii/S0021999199962629.
[10] R. Caplan, Q. Hoq, R. Carretero-González, and P. Kevrekidis, *Azimuthal modulational instability of vortices in the nonlinear schrödinger equation*, Optics Communications, 282 (2009), pp. 1399–1405, https://doi.org/https://doi.org/10.1016/j.optcom.2008.11.075, https://www.sciencedirect.com/science/article/pii/S003040180801198X.
[11] S. Chapman, M. Kavousanakis, E. Charalampidis, I. Kevrekidis, and P. Kevrekidis, *A spectral analysis of the nonlinear schrödinger equation in the co-exploding frame*, Physica D: Nonlinear Phenomena, 439 (2022), p. 133396, https://doi.org/https://doi.org/10.1016/j.physd.2022.133396, https://www.sciencedirect.com/science/article/pii/S016727892200149X.
[12] S. J. Chapman, M. Kavousanakis, I. G. Kevrekidis, and P. G. Kevrekidis, *Normal form for the onset of collapse: The prototypical example of the nonlinear schrödinger equation*, Phys. Rev. E, 104 (2021), p. 044202, https://doi.org/10.1103/PhysRevE.104.044202, https://link.aps.org/doi/10.1103/PhysRevE.104.044202.
[13] C.-A. Chen and C.-L. Hung, *Observation of universal quench dynamics and townes soliton formation from modulational instability in two-dimensional bose gases*, Phys. Rev. Lett., 125 (2020), p. 250401, https://doi.org/10.1103/PhysRevLett.125.250401, https://link.aps.org/doi/10.1103/PhysRevLett.125.250401.
[14] M. P. Coles, D. E. Pelinovsky, and P. G. Kevrekidis, *Excited states in the large density limit: a variational approach*, Nonlinearity, 23 (2010), p. 1753, https://doi.org/10.1088/0951-7715/23/8/001, https://dx.doi.org/10.1088/0951-7715/23/8/001.
[15] V. Dolean, P. Jolivet, and F. Nataf, *An Introduction to Domain Decomposition Methods*, Society for Industrial and Applied Mathematics, Philadelphia, PA, 2015, https://doi.org/10.1137/1.9781611974065, https://epubs.siam.org/doi/abs/10.1137/1.9781611974065, https://arxiv.org/abs/https://epubs.siam.org/doi/pdf/10.1137/1.9781611974065.
[16] G. Fibich, *The Nonlinear Schrödinger Equation: Singular Solutions and Optical Collapse*, vol. 192 of Applied Mathematical Sciences, Springer, New York, 2015, https://doi.org/10.1007/978-3-319-12748-4.
[17] G. Fibich, N. Gavish, and X.-P. Wang, *Singular ring solutions of critical and supercritical nonlinear schrödinger equations*, Physica D: Nonlinear Phenomena, 231 (2007), pp. 55–86, https://doi.org/https://doi.org/10.1016/j.physd.2007.04.007, https://www.sciencedirect.com/

science/article/pii/S0167278907001297.
[18] G. Fibich and G. Papanicolaou, *Self-focusing in the perturbed and unperturbed nonlinear schrödinger equation in critical dimension*, SIAM Journal on Applied Mathematics, 60 (1999), p. 183.
[19] D. J. Frantzeskakis, *Dark solitons in atomic bose–einstein condensates: from theory to experiments*, Journal of Physics A: Mathematical and Theoretical, 43 (2010), p. 213001, https://doi.org/10.1088/1751-8113/43/21/213001, https://dx.doi.org/10.1088/1751-8113/43/21/213001.
[20] A. Hasegawa and Y. Kodama, *Solitons in Optical Communications*, Clarendon Press, Oxford, 1995.
[21] F. Hecht, *New development in freefem++*, J. Numer. Math., 20 (2012), pp. 251–265, https://freefem.org/.
[22] V. T. Hoang, J. Widjaja, Y. L. Qiang, M. Liu, T. J. Alexander, A. F. J. Runge, and C. M. de Sterke, *Observation of fractional evolution in nonlinear optics*, 2024, https://arxiv.org/abs/2410.23671, https://arxiv.org/abs/2410.23671.
[23] P. G. Kevrekidis, D. J. Frantzeskakis, and R. Carretero-González, *The Defocusing Nonlinear Schrödinger Equation*, SIAM, Philadelphia, 2015.
[24] Y. S. Kivshar and G. P. Agrawal, *Optical Solitons: From Fibers to Photonic Crystals*, Academic Press, 2003, https://doi.org/10.1016/B978-0-12-410590-4.X5000-1.
[25] M. Kono and M. Skorić, *Nonlinear Physics of Plasmas*, Springer-Verlag, Heidelberg, 2010.
[26] Y. Kuznetsov, *Elements of Bifurcation Theory (4th Edition)*, Springer-Verlag (New York), 2023.
[27] M. J. Landman, G. C. Papanicolaou, C. Sulem, and P. L. Sulem, *Rate of blowup for solutions of the nonlinear schrödinger equation at critical dimension*, Phys. Rev. A, 38 (1988), pp. 3837–3843, https://doi.org/10.1103/PhysRevA.38.3837, https://link.aps.org/doi/10.1103/PhysRevA.38.3837.
[28] K. D. Moll, A. L. Gaeta, and G. Fibich, *Self-similar optical wave collapse: Observation of the townes profile*, Phys. Rev. Lett., 90 (2003), p. 203902, https://doi.org/10.1103/PhysRevLett.90.203902, https://link.aps.org/doi/10.1103/PhysRevLett.90.203902.
[29] H. Nawa, *Two points blow-up in solutions of the nonlinear schrödinger equation with quartic potential on*, Journal of Statistical Physics, 91 (1998), pp. 439–458, https://doi.org/10.1023/A:1023012709647.
[30] C. J. Pethick and H. Smith, *Bose–Einstein Condensation in Dilute Gases*, Cambridge University Press, Cambridge, second ed., 2008, https://doi.org/10.1017/CBO9780511802850.
[31] L. P. Pitaevskii and S. Stringari, *Bose-Einstein Condensation*, no. 116 in Oxford Science Publications, Clarendon Press, Oxford ; New York, 2003.
[32] C. W. Rowley, I. G. Kevrekidis, J. E. Marsden, and K. Lust, *Reduction and reconstruction for self-similar dynamical systems*, Nonlinearity, 16 (2003), p. 1257, https://doi.org/10.1088/0951-7715/16/4/304, https://dx.doi.org/10.1088/0951-7715/16/4/304.
[33] G. Sadaka, P. Jolivet, E. G. Charalampidis, and I. Danaila, *Parallel finite-element codes for the bogoliubov-de gennes stability analysis of bose-einstein condensates*, Computer Physics Communications, 306 (2025), p. 109378, https://doi.org/https://doi.org/10.1016/j.cpc.2024.109378, https://www.sciencedirect.com/science/article/pii/S0010465524003011.
[34] C. I. Siettos, I. G. Kevrekidis, and P. G. Kevrekidis, *Focusing revisited: a renormalization/bifurcation approach*, Nonlinearity, 16 (2003), pp. 497–506.
[35] A. Sukhinin, A. B. Aceves, J.-C. Diels, and L. Arissian, *Collapse events of two-color optical beams*, Phys. Rev. A, 95 (2017), p. 031801, https://doi.org/10.1103/PhysRevA.95.031801, https://link.aps.org/doi/10.1103/PhysRevA.95.031801.
[36] C. Sulem and P. Sulem, *The nonlinear Schrödinger equation: self-focusing and wave collapse*, Springer, New York, 1999.
[37] A. Toselli and O. B. Widlund, *Domain Decomposition Methods - Algorithms and Theory*, Springer-Verlag (Berlin), 2005, https://doi.org/https://doi.org/10.1007/b137868.
[38] H. Uecker, *Numerical Continuation and Bifurcation in Nonlinear PDEs*, SIAM (Philadelphia), 2021.
[39] L. T. Vuong, T. D. Grow, A. Ishaaya, A. L. Gaeta, G. W. 't Hooft, E. R. Eliel, and G. Fibich, *Collapse of optical vortices*, Phys. Rev. Lett., 96 (2006), p. 133901, https://doi.org/10.1103/PhysRevLett.96.133901, https://link.aps.org/doi/10.1103/PhysRevLett.96.133901.